1 **Landsat and Sentinel-derived glacial lake dataset in the China-**

2 **Pakistan Economic Corridor from 1990 to 2020**

4 Muchu Lesi[1], Yong Nie[1, *], Dan H. Shugar[2], Jida Wang[3], Qian Deng[1, 4], Huayong Chen[1],

5 Jianrong Fan[1]

7 [1]Institute of Mountain Hazards and Environment, Chinese Academy of Sciences, Chengdu,

8 China

9 [2]Water, Sediment, Hazards, and Earth-surface Dynamics (waterSHED) Lab, Department of

10 Geoscience, University of Calgary, Alberta, T2N 1N4, Canada

11 [3]Department of Geography and Geospatial Sciences, Kansas State University, Manhattan,
12 Kansas 66506, USA

13 [4]University of Chinese Academy of Sciences, Beijing 100190, China

17 [*]Corresponding author, nieyong@imde.ac.cn

20 **Abstract.** The China-Pakistan Economic Corridor (CPEC) is one of the flagship projects of
21 the One Belt One Road Initiative, which faces threats from water shortage and mountain
22 disasters in the high-elevation region, such as glacial lake outburst floods (GLOFs). An up-to-
23 date high-quality glacial lake dataset with parameters such as lake area, volume and type,
24 which is fundamental to water resource and flood risk assessments, and predicting glacier-
25 lake evolutions, is still largely absent for the entire CPEC. This study describes a glacial lake
26 dataset for the CPEC using a threshold-based mapping method associated with rigorous
27 visual inspection workflows. This dataset includes (1) multi-temporal inventories for 1990,
28 2000, and 2020 produced from 30 m resolution Landsat images, and (2) a glacial lake
29 inventory for the year 2020 at 10 m resolution produced from Sentinel-2 images. The results
30 show that, in 2020, 2234 lakes were derived from the Landsat images, covering a total area of
31 86.31 ± 14.98 km^2 with a minimum mapping unit of 5 pixels (4500 m^2), whereas 7560 glacial
32 lakes were derived from the Sentinel-2 images with a total area of 103.70 ± 8.45 km^2 with a
33 minimum mapping unit of 5 pixels (500 m^2). The discrepancy shows that Sentinel-2 is able to
34 detect a significant quantity of smaller lakes than Landsat due to its finer spatial resolution.
35 Glacial lake data in 2020 was validated by Google Earth-derived lake boundaries with a
36 median ($\pm$standard deviation) difference of 7.66 ± 4.96 % for Landsat-derived product and
37 4.46 ± 4.62 % for Sentinel-derived product. The total number and area of glacial lakes from
38 consistent 30 m resolution Landsat images remain relatively stable despite a slight increase
39 from 1990 to 2020. A range of critical attributes have been generated in the dataset, including
40 lake types and mapping uncertainty estimated by an improved Hanshaw's equation. This
41 comprehensive glacial lake dataset has potential to be widely applied in studies on water
42 resource assessment, glacial lake-related hazards, glacier-lake interactions, and is freely
43 available at https://doi.org/10.12380/Glaci.msdc.000001 (Lesi et al., 2022).

1 Introduction

45 Glaciers in High-mountain Asia (HMA) play a crucial role in regulating climate, supporting
46 ecosystems, modulating the release of freshwater into rivers, and sustaining municipal water
47 supplies (Wang et al., 2019; Viviroli et al., 2020), agricultural irrigation, and hydropower
48 generation (Pritchard, 2019; Nie et al., 2021). Most HMA glaciers are losing mass in the
49 context of climate change (Brun et al., 2017; Maurer et al., 2019; Shean et al., 2020;
50 Bhattacharya et al., 2021), therefore, unsustainable glacier melt and the passing of peak water
51 are reducing the hydrological role of glaciers (Huss and Hock, 2018) and impacting
52 downstream ecosystem services, agriculture, hydropower and other socioeconomic values
53 (Carrivick and Tweed, 2016; Nie et al., 2021). The present and future glacier changes not
54 only impact water supply for downstream area but also alter the frequency and intensity of
55 glacier-related hazards, such as glacier lake outburst floods (GLOFs) (Nie et al., 2018;
56 Rounce et al., 2020; Zheng et al., 2021), and rock and ice avalanches (Shugar et al., 2021).
57 Global glacial lake number and total area both increased between 1990 and 2018 in response
58 to glacier retreat and climate change (Shugar et al., 2020), affecting the allocation of
59 freshwater resource. The Indus is globally the most important and vulnerable water tower unit
60 where glaciers, lakes and reservoir storage contribute about two-thirds of the water supply
61 (Immerzeel et al., 2020). Ice-marginal lakes store ~1% of total ice discharge in Greenland and
62 accelerate lake-terminating ice velocity by ~25% (Carrivick et al., 2022). An increasing

63 frequency and risk of GLOFs (Nie et al., 2021; Zheng et al., 2021) is threatening Asian
64 population and infrastructures in the mountain ranges, such as the China-Pakistan Economic
65 Corridor (CPEC), as a flagship component of One Belt One Road Initiative (Battamo et al.,
66 2021; Li et al., 2021). The northern section of the CPEC passes through Pamir, Karakoram,
67 Hindu Kush and Himalaya mountains where droughts and glacier-related hazards are frequent
68 and severe (Hewitt, 2014; Bhambri et al., 2019; Pritchard, 2019), threatening local people,
69 the existing, under-construction and planned infrastructures, such as highways, hydropower
70 plants and railways. Understanding the risk posed by water shortage and glacier-related
71 hazards is a critical step to sustainable development for the CPEC.
72   Glacial lake inventories with a range of attributes benefit water resource assessment and
73 disaster risk assessment related to glacial lake (Wang et al., 2020; Carrivick et al., 2022), and
74 contribute to predicting glacier-lake evolution and cryosphere-hydrosphere interactions under
75 climate change (Nie et al., 2017; Brun et al., 2019; Maurer et al., 2019; Carrivick et al., 2020;
76 Liu et al., 2020). Remote sensing is the most viable way to map glacial lakes and detect their
77 spatio-temporal changes in the high-elevation zones where in situ accessibility is extremely
78 low (Huggel et al., 2002; Quincey et al., 2007). Studies in glacial lake inventories using
79 satellite observations have been heavily conducted at regional scales recently, such as in the
80 Tibetan Plateau (Zhang et al., 2015), the Himalaya (Gardelle et al., 2011; Nie et al., 2017),
81 the HMA (Wang et al., 2020; Chen et al., 2021), the Tien Shan (Wang et al., 2013), the
82 Alaska (Rick et al., 2022), the Greenland (How et al., 2021) and the northern Pakistan
83 (Ashraf et al., 2017). However, the latest glacial lake mapping in 2020 is still absent along the
84 CPEC. Among existing studies, Landsat archival images are the most widely used due to their
85 multi-decadal record of earth surface observations, reasonably high spatial resolution (30 m),
86 and publicly available distribution (Roy et al., 2014). Freely available Sentinel-2 satellite
87 images show a better potential than Landsat in glacial lake mapping and inventories due to
88 their higher spatial resolution (10 m) and a global coverage, but have only been available
89 since late 2015 (Williamson et al., 2018; Paul et al., 2020). Glacial lake inventories using
90 Sentinel-2 images are relatively scarce at regional scales, and studies of the latest glacial lake
91 mapping as well as comparisons of glacial lake dataset derived from Sentinel-2 and Landsat
92 observations are still lacking.
93   Discrepancies between various glacial lake inventories (Zhang et al., 2015; Shugar et al.,
94 2020; Wang et al., 2020; Chen et al., 2021; How et al., 2021) result from differences in
95 mapping methods, minimum mapping units, definition of glacial lakes, time periods, data
96 sources and other factors. For example, manual vectorization method was widely adopted at
97 the earlier stage for its high accuracy. However, it is time-consuming associated with high
98 labor intensity and is only practical at regional scales (Zhang et al., 2015; Wang et al., 2020).
99 Automated and semi-automated lake mapping methods, such as multi-spectral index
100 classification (Gardelle et al., 2011; Nie et al., 2017; Zhang et al., 2018; How et al., 2021),
101 have been developed to improve the efficiency of glacial lake inventories using optical
102 images, although manual modification is often unavoidable to assure the quality of lake data
103 impacted by cloud cover, mountain shadows, seasonal snow cover and frozen lake surfaces
104 (Sheng et al., 2016; Wang et al., 2017, 2018). Backscatter images from Synthetic Aperture
105 Radar (SAR) (Wangchuk and Bolch, 2020; How et al., 2021) were used to remove the impact
106 of cloud cover for lake mapping. Besides, other approaches such as hydrological sink

107 detection using DEM (How et al., 2021) and land surface temperature-based detection
108 method (Zhao et al., 2020) were also used for lake inventories. Different classification
109 methods impact the results of lake mapping and monitoring. So far, we are lacking a unified
110 standard for the classification system of glacial lakes (Yao et al., 2018). Existing
111 classification systems are generally used for their individual research purposes, mainly based
112 on the relative positions of glacial lakes and glaciers, the supply conditions of glaciers, and
113 the attributes of dams. In addition to different classification standards, the same type of
114 glacial lakes may also have different names given by different scholars. For example, ice-
115 marginal (Carrivick and Quincey, 2014; Carrivick et al., 2020), ice-contact (Carrivick and
116 Tweed, 2013) and proglacial (Nie et al., 2017) lakes all represent glacial lakes sharing the
117 boundary with glaciers. Glacier lakes in currently available datasets have been traditionally
118 categorized by their spatial relationship with upstream glaciers (Gardelle et al., 2011; Wang
119 et al., 2020; Chen et al., 2021), and classification attributes considering the formation
120 mechanism and the properties of dams are rare or incomplete in the CPEC (Yao et al., 2018;
121 Li et al., 2020). Dam type classification of glacial lakes provides a crucial attribute for
122 glacier-lake interactions and risk assessment (Emmer and Cuřín, 2021). Therefore, an up-to-
123 date glacial lake dataset with critical, quality-assured parameters (e.g. lake area, volume and
124 type) is necessary.
125   This study aims to (1) present an up-to-date glacial lake dataset in the CPEC in 2020 using
126 both Landsat 8 and Sentinel-2 images to accurately document its detailed lake distribution;
127 (2) present two historical glacial lake datasets for the CPEC to show extent in 1990 and 2000
128 using consistent 30-m Landsat images to reveal glacial lake changes at three time periods
129 (1990, 2000 and 2020); and (3) generate a range of critical attributes for glacial lake
130 inventories to benefit studies on water resource evaluation, risk assessment of GLOFs, glacier
131 –lake evolution modeling in the HMA.

2 Study area
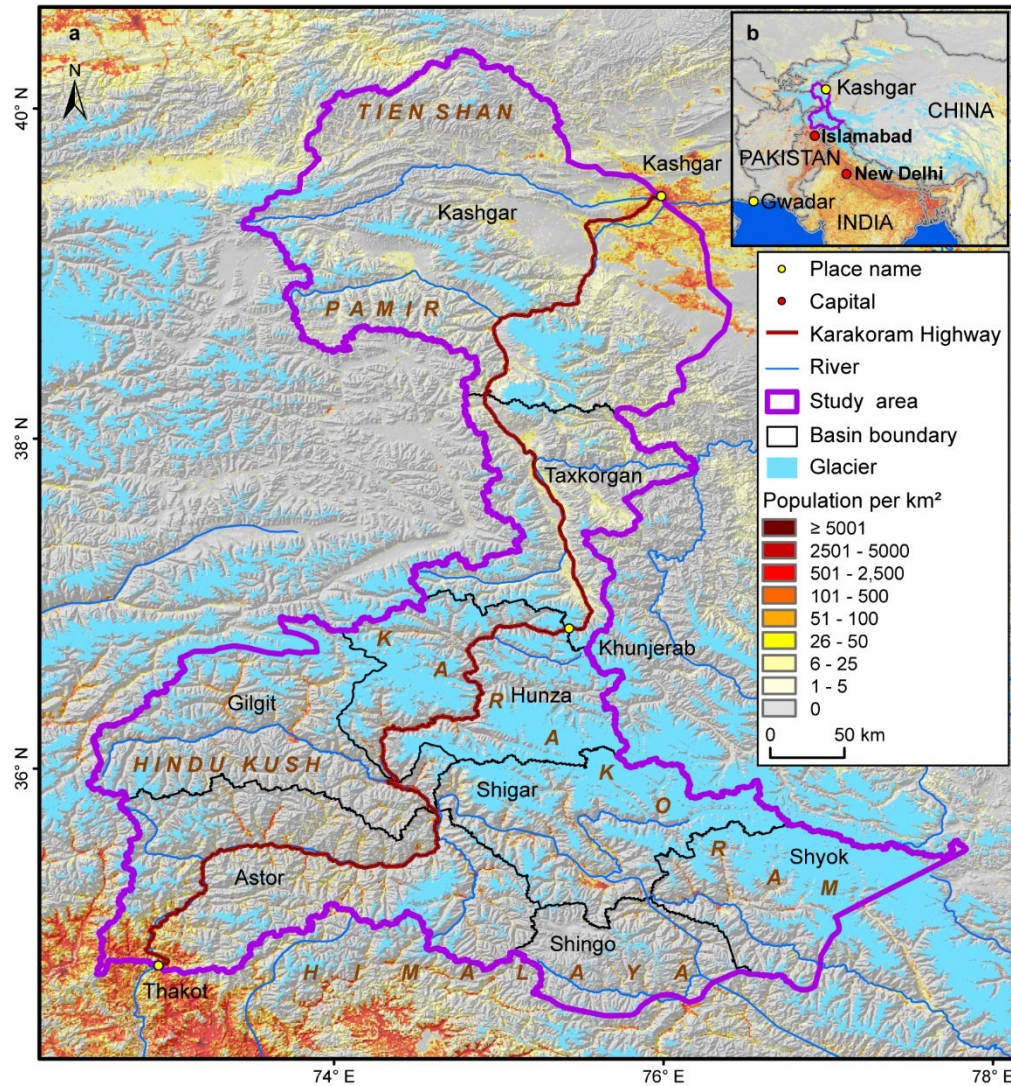
Figure 1. Location of the study area associated with distribution of glaciers (RGI Consortium, 2017), mountains, basins and population (Rose et al., 2021) (a), and its location within the CPCE (b).

The northern part of the CPEC is selected as the study area (Figure 1). The CPCE, originating from Kashgar of the Xinjiang Uygur Autonomous region, China and extending to Gwadar Port, Pakistan (Ullah et al., 2019; Yao et al., 2020), is connecting China and Pakistan via the only Karakoram Highway. The study area covers all the drainage basins along Karakoram Highway starting from Kashgar and ending at Thakot, with a total area of ~125,000 km². The upper Indus basins beyond the Pakistani-administrated border are excluded in this study due to spatial coverage of the CPCE. The entire study area is divided into eight sub-basins, covering most of the Karakoram with the highest elevation up to 8611 m, western Himalaya and Tien Shan, eastern Hindu Kush and Pamir Mountains. The 9710 glaciers in the study area cover a total area of 17,447 km² and nearly 60% of glaciers are distributed in the Karakoram (5818 glaciers with a total area of 14,067.52 km²) (RGI Consortium, 2017). Most glaciers in the western Himalaya and eastern Hindu Kush are losing mass in the context of climate change (Kääb et

149 al., 2012; Yao et al., 2012; Brun et al., 2017; Shean et al., 2020; Hugonnet et al., 2021), whereas
150 the glaciers in the eastern Karakoram and Pamir have shown unusually little changes, including
151 unchanged, retreated, advanced and surged glaciers (Hewitt, 2005; Kääb et al., 2012; Bolch et
152 al., 2017; Brun et al., 2017; Shean et al., 2020; Nie et al., 2021). The spatially heterogeneous
153 distribution and changes of glaciers are primarily explained as a result of differences in the
154 dominant precipitation-bearing atmospheric circulation patterns that include the winter
155 westerlies the Indian summer monsoon, their changing trends and their interactions with local
156 extreme topography (Yao et al., 2012; Azam et al., 2021; Nie et al., 2021).

3 Data sources

158 Both Landsat and Sentinel-2 images have been employed to map glacial lakes between 1990
159 and 2020 in the CPEC (Figure 2). A total number of 71 Landsat Thematic Mapper (TM),
160 Thematic Mapper Plus (ETM+) and Landsat 8 Operational Land Imager (OLI) images with a
161 consistent spatial resolution of 30 m were downloaded from the United States Geological
162 Survey Global Visualization Viewer (GloVis, https://glovis.usgs.gov/) to be used to create
163 glacial lake inventories in 1990, 2000 and 2020. High-quality Landsat-5 images around 2010
164 are insufficient to cover the entire study area, so we were unable to map lakes in 2010 due to
165 Landsat-7's scan-line corrector errors and significant cloud covers. In addition, 39 Sentinel-2
166 images (23 scenes in 2020) were downloaded from Copernicus Open Access Hub
167 (https://scihub.copernicus.eu/) to produce the 10-m resolution glacial lake inventory in 2020.
168 All images used in this study have been orthorectified before download, but we still find that
169 one Sentinel-2 image was not well matched with Landsat images, leading to the discrepancy
170 between the two glacial lake datasets. We manually georeferenced the shifted image to
171 minimize the difference between Sentinel and Landsat derived glacial lakes.
172   Cloud and snow covers heavily affect the usability of optical satellite images (Wulder et
173 al., 2019) and their availability in the entire study area, so we took advantage of the images
174 acquired before and after each of the baseline years 1990, 2000 and 2020 to construct the
175 glacial lake inventories. Only 4 images in 1990 (the largest covering the study area), 16
176 images in 2000 and 23 images in 2020 were used for matching baseline year. Spatially, high-
177 quality images in given baseline years were preferentially chosen, or we selected one or more
178 alternative images acquired in adjacent years to delineate glacial lakes by removing the effect
179 of cloud and snow covers. To minimize the impact of intra-annual changes of glacial lakes,
180 most of used images (82% for Sentinel-2 and 75% for Landsat) were acquired from August to
181 October in the given baseline year with cloud coverage of <20% for each image. For some
182 specific scenes where cloud cover exceeded the threshold of 20%, we selected more than one
183 image to remedy the effect of cloud contamination (Nie et al., 2010, 2017; Jiang et al., 2018).
184   Other datasets used include the Randolph Glacier Inventory version 6.0 (Pfeffer et al.,
185 2014; RGI Consortium, 2017) and the Glacier Area Mapping for Discharge from the Asian
186 Mountains (GAMDAM) glacier inventory (Sakai, 2019). These two glacier datasets were
187 used to determine glacial lake types, such as ice-contact, ice-dammed and unconnected-
188 glacier-fed lakes. The Shuttle Radar Topography Mission Digital Elevation Model (SRTM
189 DEM) at a 1-arc second (30 m) resolution (Jarvis et al., 2008) was employed to extract the
190 altitudinal characteristics of the glacial lakes. The absolute vertical accuracy of the SRTM
191 DEM is 16 m (90%) (Rabus et al., 2003; Farr et al., 2007). We also applied other published

192 glacial lake datasets for comparative analysis. They include the glacial lake inventories of
193 HMA in 1990 and 2018 downloaded from http://doi.org/10.12072/casnw.064.2019.db (Wang
194 et al., 2020), the Third Pole region in 1990, 2000 and 2010 publicly shared at
195 http://en.tpedatabase.cn/ (Zhang et al., 2015), the Tibet Plateau from 2008 to 2017 accessed at
196 https://doi.org/10.5281/zenodo.3700282 (Chen et al., 2021), and the entire world in 1990,
197 2000 and 2015 provided at https://nsidc.org/data /HMA_ GLI/versions/1 (Shugar et al.,
198 2020). In addition, field survey data collected between 2017 and 2018 were also used to assist
199 in lake mapping and glacial lake type classification.
200

201
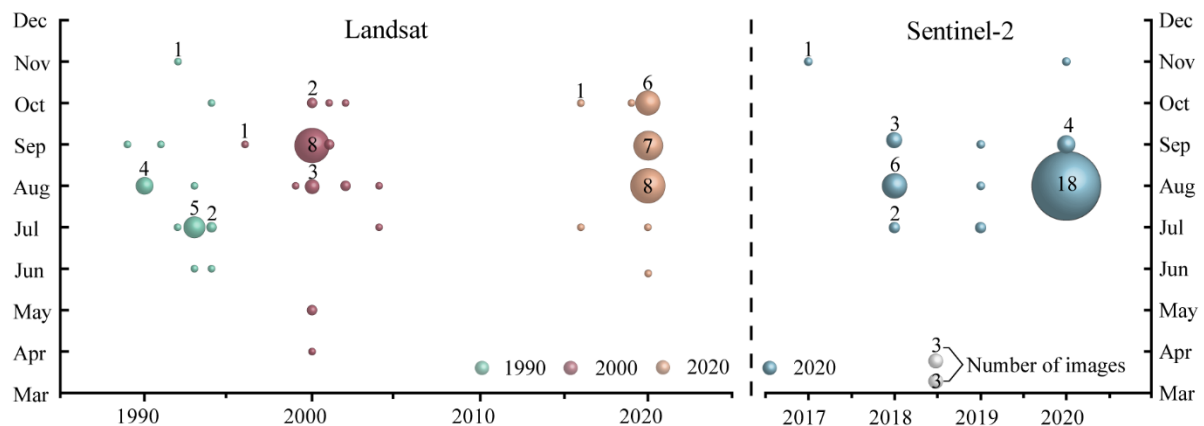
202 **Figure 2.** Acquisition years and months of Landsat and Sentinel-2 images selected for glacial lake
203 inventories. The bubble size indicates the available high-quality image number.

4 Glacial lake inventory methods

4.1 Definition of glacial lakes

206 We consider a glacial lake as one that formed as a result of modern or ancient glaciation.
207 Contemporary glacial lakes are easily recognized using a combination of glacier inventories
208 and remote sensing images. Ancient glacial lakes can be identified from periglacial
209 geomorphological characteristics, including moraine remnants and U-shaped valleys that are
210 discernible from satellite observations (Post and Mayo, 1971; Westoby et al., 2014; Nie et al.,
211 2018; Martín et al., 2021). A 10-km buffering distance of RGI 6.0 glacier boundaries that has
212 been widely used in previous studies (Zhang et al., 2015; Wang et al., 2020), was created to
213 help mapping glacial lakes. A few glacial lakes in the study area (a total of 84 lakes for
214 Sentinel-2 dataset and 55 lakes for Landsat dataset in 2020) beyond the buffering zone,
215 located near buffering boundaries, were intentionally included due to clear evidence of
216 glaciation (Figure 3). Landslide-dammed lakes (Chen et al., 2017) in the buffering zone were
217 excluded in our inventories because of their irrelevance to glaciation. All glacial lakes in the
218 study area were mapped according to our definition. We were able to implement this
219 definition by carefully leveraging the spectral properties of glacial lakes and the periglacial
220 geomorphological features that are often evident in remote sensing images (see more in
221 sections 4.3 and 4.4).
222
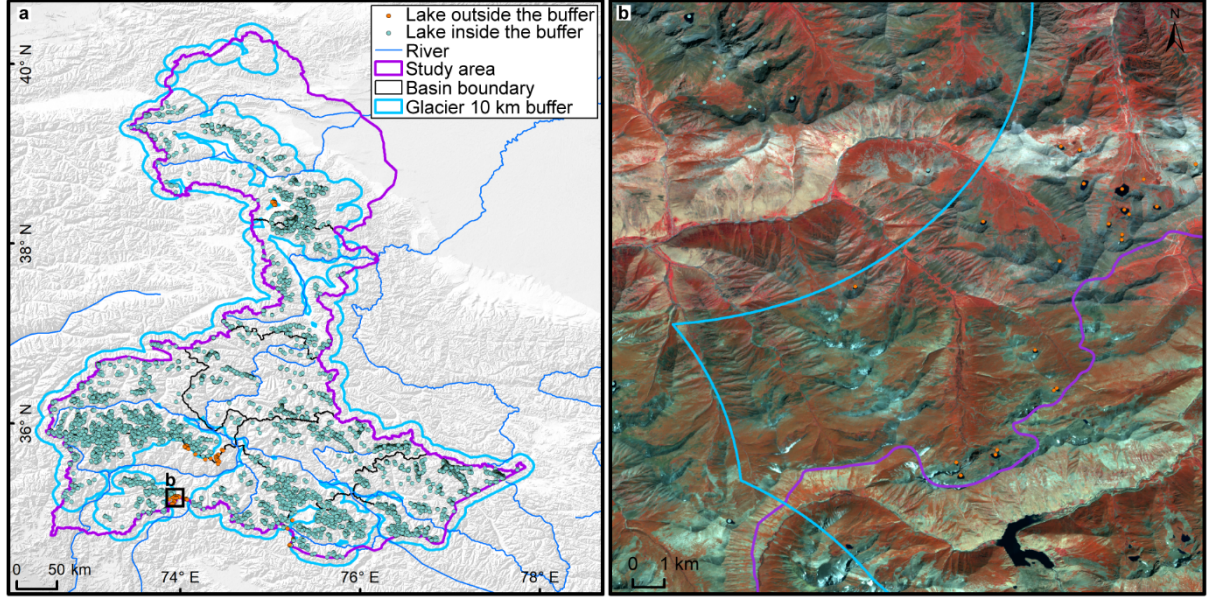
Figure 3. The 10-km buffer zone of RGI 6.0 glacier boundaries (a) and Sentinel-derived glacial lakes located near buffering boundary within the study area (b).

4.2 Interactive lake mapping

A human-interactive and semi-automated lake mapping method (Wang et al., 2014; Nie et al., 2017, 2020) was adopted to accurately extract glacial lake extents using Landsat and Sentinel-2 images, based on the Normalized Difference Water Index (NDWI) (Mcfeeters, 1996). The NDWI uses the green and near infrared bands and is calculated by the following equation:

$$NDWI = \frac{Band_{Green} - Band_{NIR}}{Band_{Green} + Band_{NIR}} \tag{1}$$

where the green band and near infrared band were provided by both Landsat and Sentinel multispectral images.

Specifically, the method calculated the NDWI histogram based on the pixels with each user-defined and manually-drawn region of interest. The NDWI threshold that separates lake surface from land was interactively determined by screening the NDWI histogram against the lake region in the imagery (Wang et al., 2014; Nie et al., 2020). This way, the determined NDWI threshold can be well-tuned to adapt various spectral conditions of the studied glacier lakes. The raster lake extents segmented by the thresholds were then automatically converted to vector polygons. We first completed the glacial lake inventory in 2020 using this interactive mapping method, and the 2020 inventory was then used as a reference to facilitate the lake mapping for other periods.

The minimum mapping unit (MMU) was set to 5 pixels for both Landsat (0.0045 km^2) and Sentinel-2 images (0.0005 km^2) in this study. MMU determines the total number and area of glacial lakes in the dataset, and varies in the previous studies, such as 3 pixels (Zhang et al., 2015), 6 pixels (Wang et al., 2020), or 9 pixels (Chen et al., 2021) for a regional scale, or 55 pixels (Shugar et al., 2020) for a global scale. While a smaller threshold leads to a large quantity of lakes mapped, it also generates larger mapping noises or uncertainties.
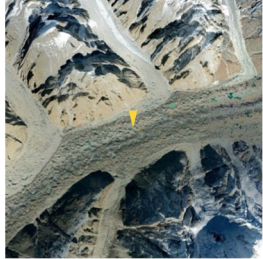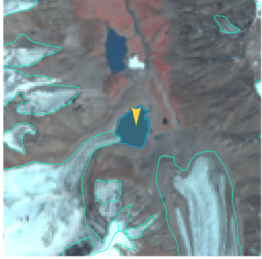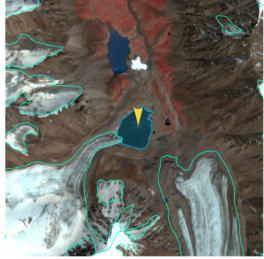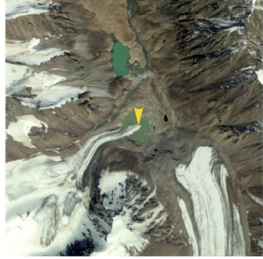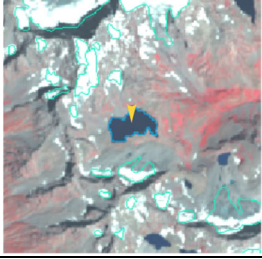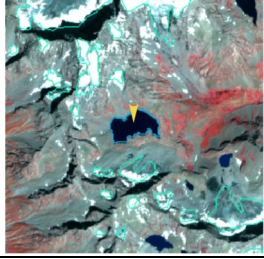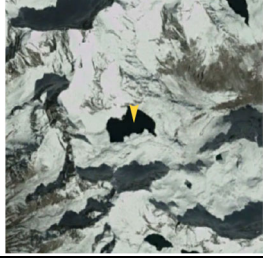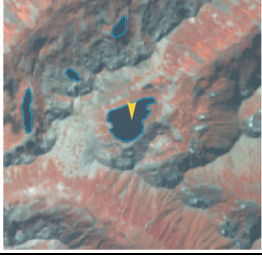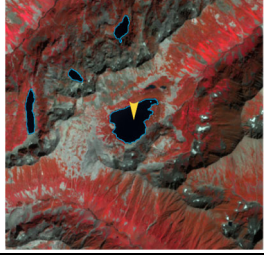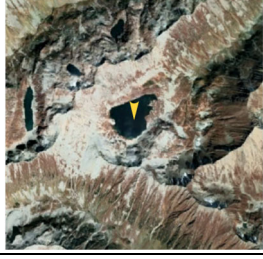
251 Considering this signal-noise balance and our focus on identifying prominent glacier lake
252 dynamics in the study area, we opted to use 5 pixels as the MMU for both Landsat and
253 Sentinel-2 images.
254   Several procedures were taken to assure the quality assurance and quality control for lake
255 mapping, including 1) visual inspection and modification using the threshold-based mapping
256 method for each lake according to Landsat, Sentinel-2 and Google Earth high-resolution
257 images overlaying preliminarily lake boundary extraction at the given time period; 2) time
258 series check for Landsat-derived glacial lake datasets from 1990 and 2020, and cross-check
259 between Landsat and Sentinel-2-derived lake dataset in 2020 to reduce errors of omission and
260 commission; 3) topological validation of glacial lake mapping, such as repeated removal,
261 elimination of small sliver polygons; and 4) logical check for lake types between two
262 classification systems of glacial lakes. False lake extents resulting from cloud or snow cover,
263 lake ice, and topographic shadows (Nie et al., 2017, 2020) were modified using previous
264 semi-automated mapping method based on alternative images acquired in adjacent years.
265 Those procedures were time-consuming, but helped to minimize the effect of cloud and snow
266 covers, lake mapping errors, and to maximize the quality of the produced lake product and
267 the derived glacial lake changes.

268 4.3 Classification of glacial lakes
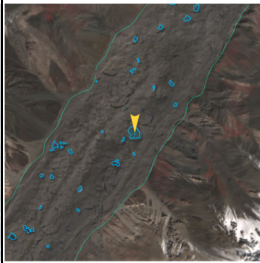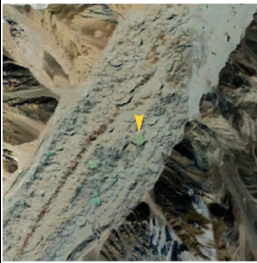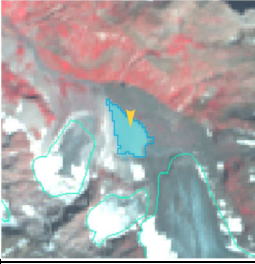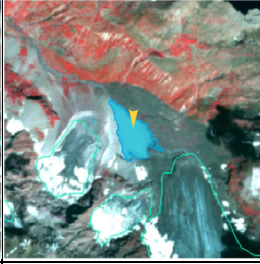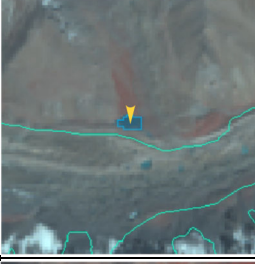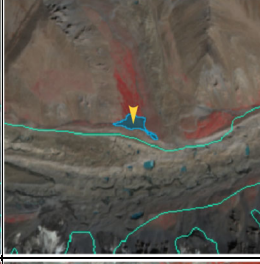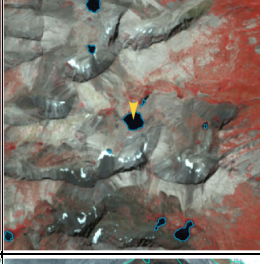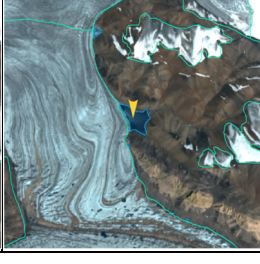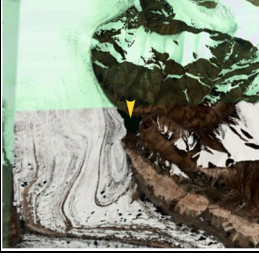
269 Two glacial lake classification systems (GLCS) have been established based on relationship
270 of interaction between glacial lakes and glaciers as well as lake formation mechanism and
271 dam material properties. In the first GLCS (GLCS1), glacial lakes were classified into four
272 types based on their spatial relationship to upstream glaciers: supraglacial, ice-contact,
273 unconnected-glacier-fed lakes, and non-glacier-fed lakes according to Gardelle et al. (2011)
274 and Carrivick et al. (2013). Alternatively, combining the formation mechanism of glacial
275 lakes and the properties of natural dam features, glacial lakes were classified into five
276 categories (herein named GLCS2) modified from Yao's classification system (2018):
277 supraglacial, end-moraine-dammed, lateral-moraine-dammed, glacial-erosion lakes and ice-
278 dammed lakes. Subglacial lakes were excluded due to the mapping challenge from spectral
279 satellite images alone. Characterization and examples for each type are provided in Table 1
280 and Table 2. Individual glacial lakes were categorized to the specific types for each GLCS
281 according to available glacier inventory data, geomorphological and spectral characteristics
282 interpreted from Landsat, Sentinel and Google Earth images. The synergy of these two
283 GLCSs is beneficial to predicting glacier-lake evolutions and providing fundamental data for
284 water resource and glacial lake disaster risk assessment.
285

286

Table 1. Classification system of glacial lake types (GLCS1) according to the relationship between glacial
lakes and glaciers (© Google Earth 2019). Glacier outlines are from RGI 6.0 (RGI Consortium, 2017), and
the yellow marker represents target lake.

Lake types	Characteristics	Landsat	Sentinel-2	Google Earth
Supraglacial	Lakes formed on the surface of glaciers, generally dammed by ice and thin debris. Case location: 35°43'49.74" N 76°13'53.88" E			
Ice-contact	Lakes dammed by moraine, ice or bedrock, supplied by glacial meltwater and shared boundary with glaciers. Case location: 39°09'32.40" N 73°43'12.00" E			
Unconnected-glacier-fed	Lakes currently supplied by upstream glacial meltwater but disconnected with glaciers. Case location: 35°47'60.00" N 72°55'15.60" E			
Non-glacier-fed	Lakes formed by glaciology, dammed by moraine or bed rock, and currently not supplied by glacial meltwater. Case location: 34°50'39.99" N 74°48'29.31" E			

290

Table 2. Classification system of glacial lake types (GLCS2) according to the formation mechanism of glacial lakes and dam material properties (© Google Earth 2019). Glacier outlines from RGI 6.0 (RGI Consortium, 2017), and the yellow marker represents target lake.

Lake types	Characteristics	Landsat	Sentinel-2	Google Earth
Supraglacial	Lakes formed on the surface of glaciers, generally dammed by ice and thin debris. Case location: 36°46'7.39" N 74°20'7.59" E			
End-moraine-dammed	Lakes formed behind moraines as a result of glacier retreat and downwasting. Case location: 35°42'50.40" N 73°09'57.60" E			
Lateral-moraine-dammed	Lakes formed behind lateral glacial moraine ridges and dammed by debris, different from ice-dammed glacial lake. Case location: 38°28'45.62" N 75°20'52.30" E			
Glacial-erosion	Lakes formed in depressions created by glacial over-deepening. Bedrock dam dominates, partially superimposed by top moraine in rugged terrain. Dams are unclear in the satellite images. Case location: 35°55'55.56" N 73°38'20.13" E			
Ice-dammed	Lakes formed behind glaciers, dammed by glacier ices (partially covered by debris on the top). Case location: 35°28'31.32" N 77°30'46.81" E			

4.4 Attributes of glacial lake data

A total of 18 attribute fields were input into our glacial lake datasets (Table 3). They include lake location (longitude and latitude), lake elevation (centroid elevation), orbital number of the image source, image acquisition date, lake area, lake perimeter, lake types of the two GLCSs, mapping uncertainty, lake water volume and the country, sub-basin, and mountain range associated with the lake. Amongst the attributes, lake location was calculated based on the

centroid of each glacial lake polygon associated with the DEM, N represents northing and E represents easting. Orbital number of the image source was filled with the corresponding satellite image, with the codes expressed as "PxxxRxxx" or "Txxxxx", where P and R indicate the path and row for Landsat image and T represents the tile of Sentinel-2 image associated with 5 digit code of military grid reference system. SceneID indicated identifying information of image source for Landsat or Sentinel-2, consisted of the orbital number, sensor ID and acquisition date (YYYYMMDD) for Landsat image, or the orbital number and acquisition date (YYYYMMDD) for Sentinel-2 image. Area and perimeter were automatically calculated based on glacial lake extents. Lake water volume was estimated by area-volume empirical equation (Cook and Quincey, 2015). Lake types were attributed using the characterization and interpretation marks described in Section 4.3. Mapping uncertainty was estimated using our modified equation which will be introduced in section 4.5 and appendix tutorial. Located country, sub-basin and mountain range of each glacial lake was identified by overlapping the geographic boundaries of countries, basins and mountain ranges.

Table 3. Attributes of glacial lake dataset.

Field Name	Type	Description	Note
FID or OBJECTID	Object ID	Unique code of glacial lake	Number
Shape	Geometry	Feature type of glacial lake	Polygon
Latitude	String	Latitude of the centroid of glacial lake polygon	Degree minute second
Longitude	String	Longitude of the centroid of glacial lake polygon	Degree minute second
Elevation	Double	Elevation of the centroid of glacial lake polygon	Unit: meter above sea level
SceneID	String	Scene ID of image source for Landsat or Sentinel-2	PxxxRxxx_xxxDYYYYMMDD or Txxxxx_YYYYMMDD
ACQDATE	String	Acquisition date of source image	YYYYMMDD
GLCS1	String	The first classification system of glacial lakes based on relationship of interaction between glacial lakes and glaciers	Supraglacial, Ice-contact, Unconnected-glacier-fed, None-glacier-fed

Field Name	Type	Description	Note
GLCS2	String	The second classification system of glacial lakes based on lake formation mechanism and dam material properties	Supraglacial, End-moraine-dammed, Lateral-moraine-dammed, Glacial-erosion and Ice-dammed
Basin	String	Basin name where glacial lake locates in	
Mountain	String	Mountain name where glacial lake locates in	
Country	String	Country name where glacial lake locates in	
Perimeter	Double	Perimeter of glacial lake boundary	Unit: meter
Area	Double	Area of glacial lake coverage	Unit: square meter
AreaUncer	Double	Area uncertainty of glacial lake mapping estimated based on modified Hanshaw's equation (2014)	Unit: square meter
Operator	String	Operator of glacial lake dataset	Muchu, Lesi
Examiner	String	Examiner of glacial lake dataset	Yong, Nie
Volume	Double	Water volume of glacial lake estimated by area-volume empirical equation	Unit: cubic meter

317

318   4.5 Error and uncertainty assessment

319   4.5.1 Improved uncertainty estimating method

320   We modified Hanshaw's (2014) equation that had been used to calculate lake-area mapping
321   uncertainty. Lake perimeter and displacement error are widely used to estimate the
322   uncertainty of glacier and lake mapping from satellite observation (Carrivick and Quincey,
323   2014; Hanshaw and Bookhagen, 2014; Wang et al., 2020). Hanshaw and Bookhagen (2014)
324   proposed an equation to calculate the error of area measurement by the number of edge pixels
325   of the lake boundary multiplied by half of a single pixel area. The number of edge pixels is
326   simply calculated by the perimeter divided by the grid size. The equation is expressed as
327   below:

328    $$Error(1\sigma) = \frac{P}{G} \times 0.6872 \times \frac{G^2}{2} \qquad (2)$$

329    $$D = \frac{Error(1\sigma)}{A} \times 100\% \qquad (3)$$

330   Where G is the cell size of the remote sensing imagery (10 m for Sentinel-2 image and 30 m
331   for Landsat image). P is the perimeter of individual glacial lake (m), and the coefficient of
332   0.6872 (1σ), which means nearly 69% of the edge pixels are subject to errors (Hanshaw and
333   Bookhagen, 2014), was chosen assuming that area measurement errors follow a Gaussian
334   distribution. Relative error (D) was calculated by equation 3, in which A is the area of an
335   individual glacial lake.
336   In the original equation 2, the number of edge pixels varies by the shape of lake and is

337   indicated by $\frac{P}{G}$. However, the pixels in the corner are double counted (Figure 4). The total

338   number of repeatedly calculated edge pixels equals the number of inner nodes. Therefore, we
339   adjusted the calculation of the actual number of edge pixels as the maximum of edge pixels

340   ($\frac{P}{G}$) subtracting the number of inner nodes. Accordingly, the equation of uncertainty

341   estimation for lake mapping is modified as below:

342    $$Error(1\sigma) = (\frac{P}{G} - N_{Inner}) \times 0.6872 \times \frac{G^2}{2} \qquad (4)$$

343   Where N_{Inner} is the number of inner nodes (inflection points) of each lake. The modified
344   equation is also suitable for lakes with islands (as illustrated in Figure 4b).
345   For polygons without islands (Figure 4a), use the following equation:

346    $$N_{Inner} = (\frac{N_{Total} - 4 - 1}{2}) \qquad (5)$$

347   N_{Total} is the total number of nodes, including both the outer and inner. N_{Total} is calculated
348   by the "Field Calculator" in ArcGIS, in some cases, it is necessary to remove the redundant
349   nodes before calculating the total number of nodes (See the Appendix for more details). An
350   inner node is a polygon vertex where the interior angle surrounding it is greater than 180
351   degrees. An outer node is the opposite of the inner node, where the interior angle is less than
352   180 degrees. We found that the outer nodes are usually four more than the inner nodes in our

glacial lake dataset. The total nodes in ArcGIS contain one overlapping node to close the polygon, meaning the endpoint is also the startpoint. This extra count was deleted in the calculation (equation 5).

For polygons with island (Figure 4b) use the following equation:

$$N_{Inner} = (\frac{N_{Total} - (N_{Island} + 1) \times 5}{2})$$ (6)

N_{Island} is the number of islands within each polygon. A calculation method of N_{Island} is given in the Appendix.
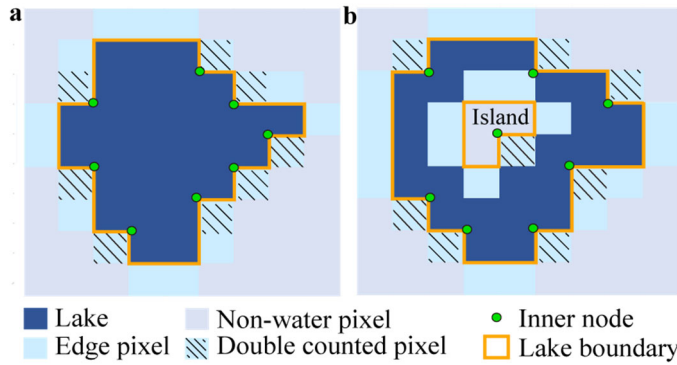
Figure 4. Sketch of estimating the actual edge pixels for uncertainty calculation of individual glacial lake (with (a) and without islands (b)).

4.5.2 Validation of glacial lake mapping

A total of 89 glacial lakes were selected by stratified random sampling and manually digitized based on the Google Earth images in circa 2020 with a spatial resolution of ～2 m acquired from WorldView, GeoEye, Pleiades etc. satellites to further validate the absolute error of our glacial lake products in 2020 due to lacking of field measurements for glacial lakes in the study area. During the sampling, we set a minimum lake area to be 4500 m^2 and a relative difference between Landsat- and Sentinel-derived lake areas less than 18% (nearly equaling to the average relative error of ±17.36% for Landsat lake mapping) in order to minimize the effect of lake changes from multi-temporal satellite observations in circa 2020. The 89 sample lakes range from 0.005 km^2 to 0.802 km^2 with a median (standard deviation) size of 0.047±0.134 km^2 and a total area of 8.033 km^2 for Landsat-derived dataset, and range from 0.005 km^2 to 0.849 km^2 with a median (standard deviation) size of 0.045±0.144 km^2 and a total area of 8.447 km^2 for Sentinel-derived dataset.

5 Results

5.1 Glacier lake distribution and changes observed from Landsat

We mapped 2,234 glacial lakes for 2020 across the studied CPEC from Landsat-8 images, with a total area of 86.31±14.98 km^2 (Figure 5a and b). Unconnected-glacier-fed lakes are

dominant in the first classification system, followed by non-glacier-fed lakes (Figure 6) whereas glacial-erosion lakes dominate at both number (1478) and area (57.02 km^2) in the second classification system (Figure 7), followed by end-moraine-dammed lakes and supraglacial lakes. Among the classified lakes, 137 are ice-contact lakes and cover an area of 5.56 km^2, implying a higher mean size of ice-contact lakes than supraglacial lakes.

Figure 5. Distribution of glacial lakes in 2020 extracted from Landsat (a, b) and Sentinel-2 (c, d) images. Panels a and c are classified by GLCS1, and GLCS2 for sub-graph b and d.
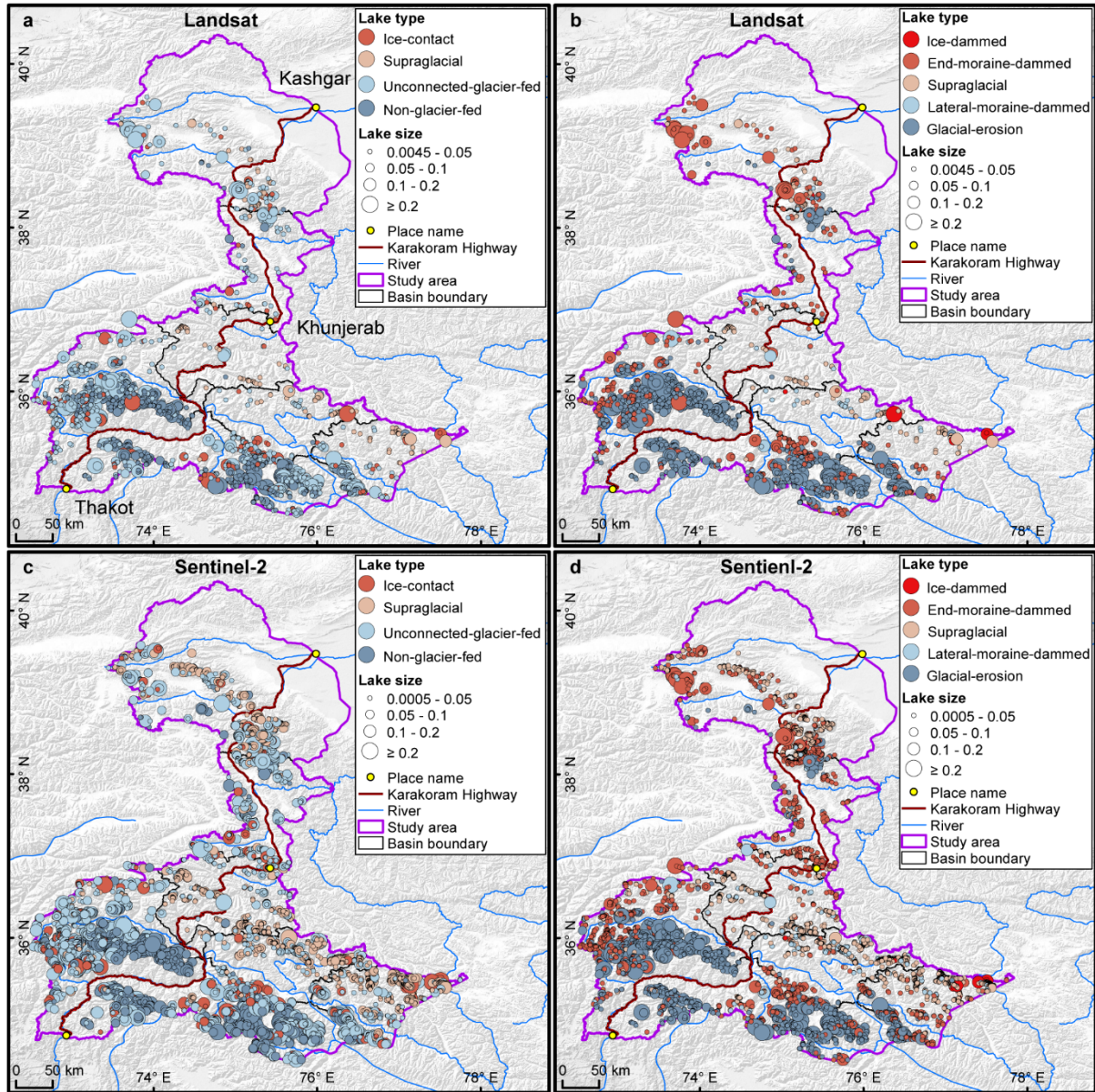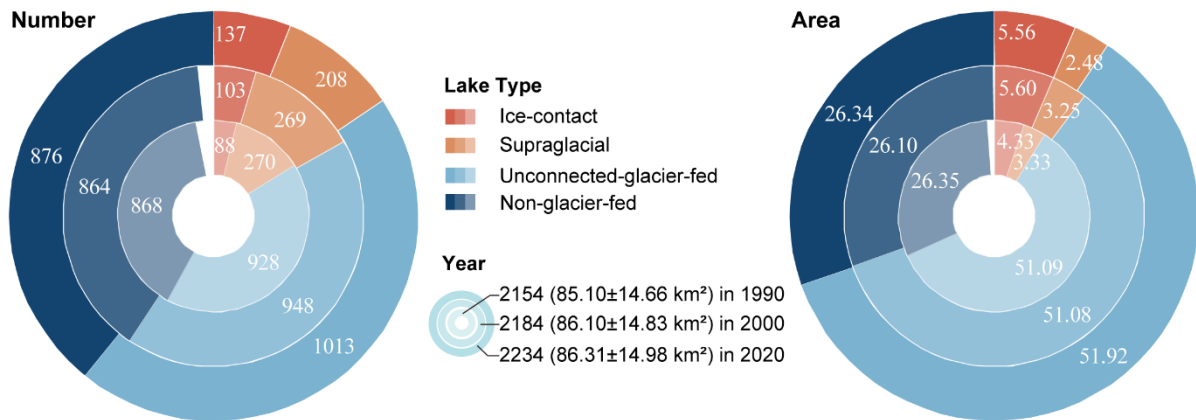
Figure 6. Number and area of different types of glacial lakes classified based on the condition of glacier supply in the study area (GLCS 1). The outermost ring represents glacial lake data in 2020, middle ring for 2000 and innermost ring for 1990. Lake number and area in 2020 were selected as reference, meaning a concept of "100 %" for a complete ring. Labeled values are scaled in degrees rather the radius of rings.
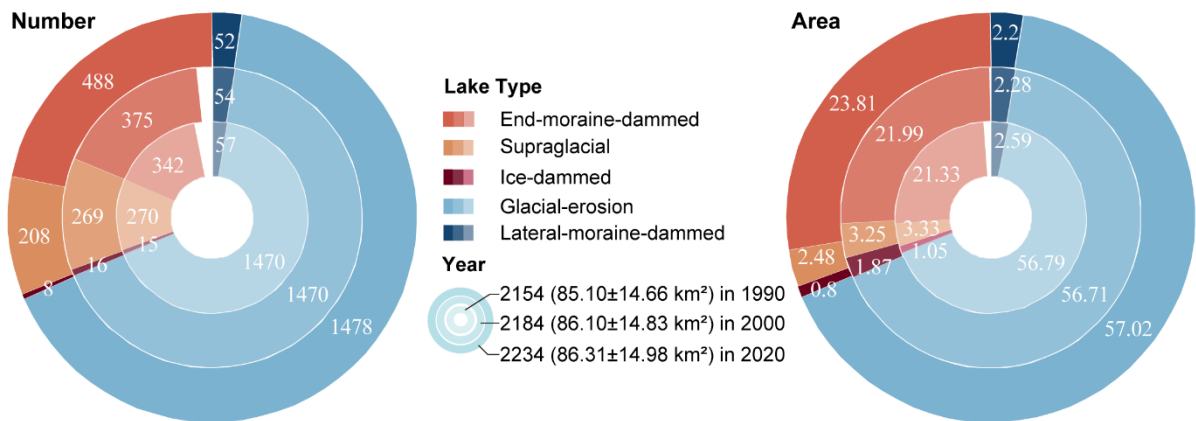
Figure 7. Number and area of different types of glacial lakes classified based on glaciation and nature of dam in the study area (GLCS 2). The outermost ring represents glacial lake data in 2020, middle ring for 2000 and innermost ring for 1990. Lake number and area in 2020 were selected as reference, meaning a concept of "100 %" for a complete ring. Labeled values are scaled in degrees rather the radius of rings.

The total number and area of glacial lakes in the study remain relatively stable with a slight increase between 1990 and 2020, and the changes in count and area among various types of glacial lakes vary substantially (Figure 6 and Figure 7). From 1990 to 2020, the total number of glacial lakes increased by 80 or 3.70%, while the area grew by 1.21 km² (or 1.42%). In GLCS1, unconnected-glacier-fed lakes have the largest increase in number, followed by ice-contact and non-glacier-fed lakes, whereas supraglacial lakes decreased by 62 in count. Ice-contact lakes expanded by 1.24 km² (equaling an increase of 26% in ice-contact lakes), contributed one third of the total area increase. Supraglacial lakes decreased by 0.85 km² in area whereas the areas of unconnected-glacier-fed and non-glacier-fed lakes remained stable as a result of disconnections from glaciers (Figure 6). In GLCS2, end-moraine-dammed lakes increased by 2.48 km² and contributed most of the glacier lake area expansion, whereas supraglacial, ice-dammed and lateral-moraine-dammed lakes decreased

417 slightly in both number and area. Glacial-erosion lakes accounted for the maximum
418 percentage (about 66% for both count and area) in each time period and remained stable
419 (Figure 7).

420 5.2 Glacier lake distribution observed from Sentinel-2

421 Sentinel-derived results shows that there are 7,560 glacial lakes (103.70±8.45 km^2) in 2020
422 across the entire CPEC (Table 4) under a MMU of 5 pixels (500 m^2). Compared with
423 Landsat-derived product, glacial lakes from Sentinel-2 have similar spatial distribution
424 characteristics (Figure 5); meanwhile, a larger quantity of glacier lakes, with more accurate
425 boundaries and a greater total lake area, were generated from Sentinel-2 images. The smallest
426 size class (0.0005-0.0045 km^2) contains the maximum lake number (4,969) but the least lake
427 area (7.73±2.62 km^2) (Table 4), which is not available in the Landsat-derived lake data due to
428 a coarser spatial resolution. In each size class, there are also a higher number of larger glacial
429 lakes from Sentinel than that from Landsat images. The discrepancy is mainly attributed to
430 the inconsistency of spatial resolutions and image acquisition dates.
431
432 **Table 4.** Count and area of glacial lakes mapped from Sentinel-2 and Landsat images in 2020 between
433 various size classes.

Lake size km^2	Glacial lakes from Sentinel-2 count (km^2)	Glacial lakes from Landsat count (km^2)	Overlap % (%)
0.0005-0.0045	4969 (7.73±2.62)	—	—
0.0045-0.05	2182 (35.52±3.72)	1870 (31.47±9.57)	85.70 (88.60)
0.05-0.1	237 (16.37±0.89)	204 (14.07±2.18)	86.08 (85.95)
0.1-0.2	122 (16.88±0.68)	115 (15.91±1.83)	94.26 (94.25)
≥0.2	50 (27.20±0.54)	45 (24.86±1.40)	90.00 (91.40)
Total	7560 (103.70±8.45)	2234 (86.31±14.98)	—

434 Note: Overlap % (%) represent the rates in count and area calculated by dividing Landsat-derived lake data by Sentinel-
435 derived data in the same size class respectively.

6 Discussions

437 6.1 Uncertainty and error of lake mapping

438 The uncertainty estimated from our improved equation shows that the relative error of
439 individual glacial lake decreases when lake size increases or cell size of remote sensing
440 images reduces (Lyons et al., 2013; Carrick and Quincey, 2014) (Figure 8). Total area
441 errors of glacial lakes in study area are approximate ±14.98 km^2 and ±8.45 km^2 in 2020 for
442 Landsat and Sentinel-2 dataset, respectively, and the average relative errors are ±17.36% and
443 ±8.15%. Generally, small lakes have greater relative errors. For example, the mean relative
444 error is 35.38% for Landsat derived glacial lakes between 0.0045 and 0.1 km^2 and 10.63% for
445 glacial lakes greater than 0.1 km^2. The mean area error of Sentinel-derived glacial lakes is
446 almost one third of that extracted from Landsat images for glacial lakes of all or specific size
447 groups. Because the relative error was estimated as a function of satellite image spatial

448 resolution and lake perimeter, the calculated error for large lake is proportionally smaller than
449 that of small lake (Salerno et al., 2012) and the error for Landsat-derived lake is naturally
450 greater than that of Sentinel-derived lake at the same size group.
451
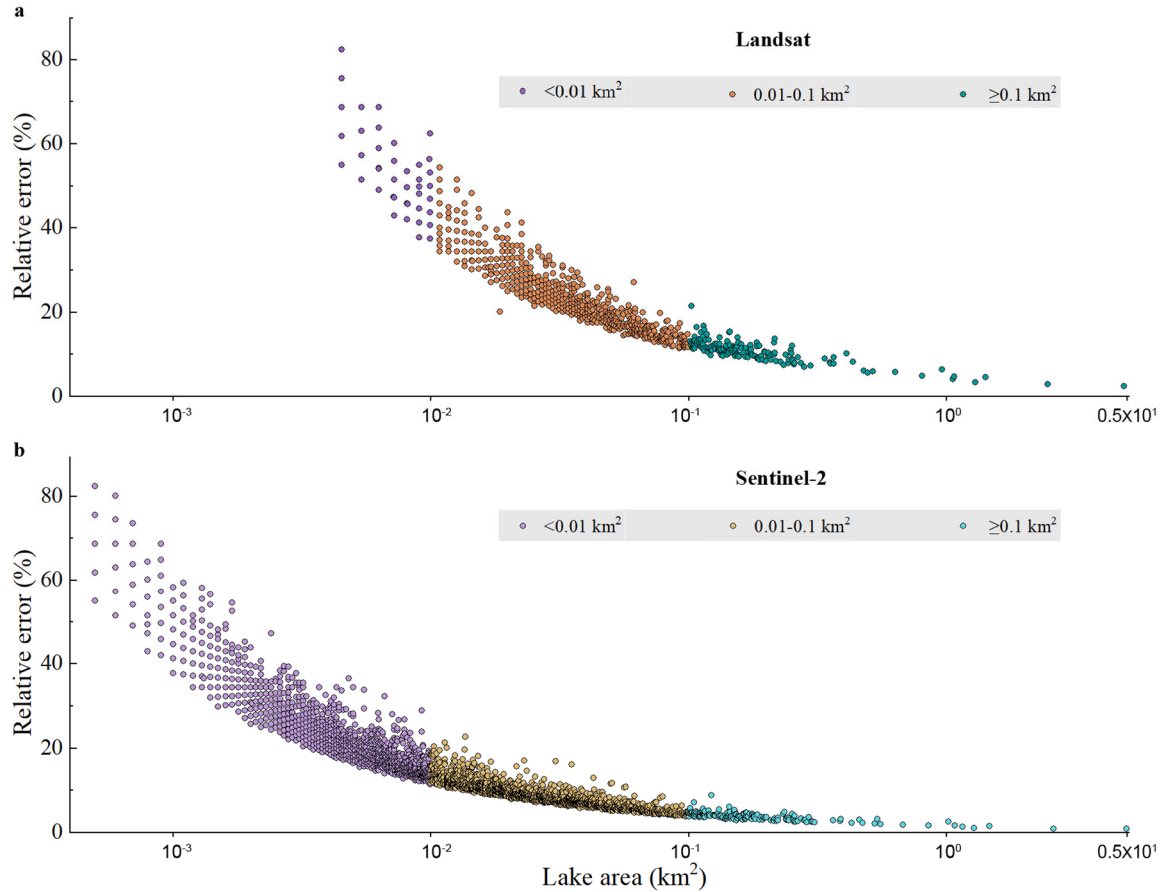
452
453 **Figure 8.** Estimated relative error for glacial lakes of all or specific size ranges in study area. Error
454 estimation is based on the modified equation and lake data extracted from Landsat (a) and Sentinel-2
455 images (b).
456
457 Our Landsat- and Sentinel-derived glacial lake dataset match well lake boundaries in Google
458 Earth higher resolution images (Figure 9). The mean difference in area is 0.005 km^2 between
459 Landsat and Google Earth derived lakes and 0.001 km^2 between Sentinel-2 and Google Earth
460 derived lakes, and major validation samples (84/89) are within the confidence interval of
461 95%, indicating a high accuracy in lake mapping (Figure 9c and d). The error of 89 sample
462 lakes is 5.48% in total area between Landsat- and Google Earth-derived data, and 0.61% for
463 Sentinel- and Google Earth-derived data. The median (±standard deviation) in discrepancy of
464 individual lake area is 7.66±4.96 % for Landsat- and Google Earth-derived data, and
465 4.46±4.62 % for Sentinel- and Google Earth-derived data. Our glacial lake dataset shows a
466 satisfactory mapping accuracy, although Sentinel-derived lake data performs more accurate
467 than those from Landsat images. We also validated the sampling Landsat-derived 89 lakes by
468 the existing Landsat-extracted lake data produced by Wang et al. (2020). A total of 83 lakes
469 are available in Wang's data with a mean difference of 0.005 km^2 in lake area (Figure A8).
470 This also shows an improvement of our lake product in contrast to the existing dataset.
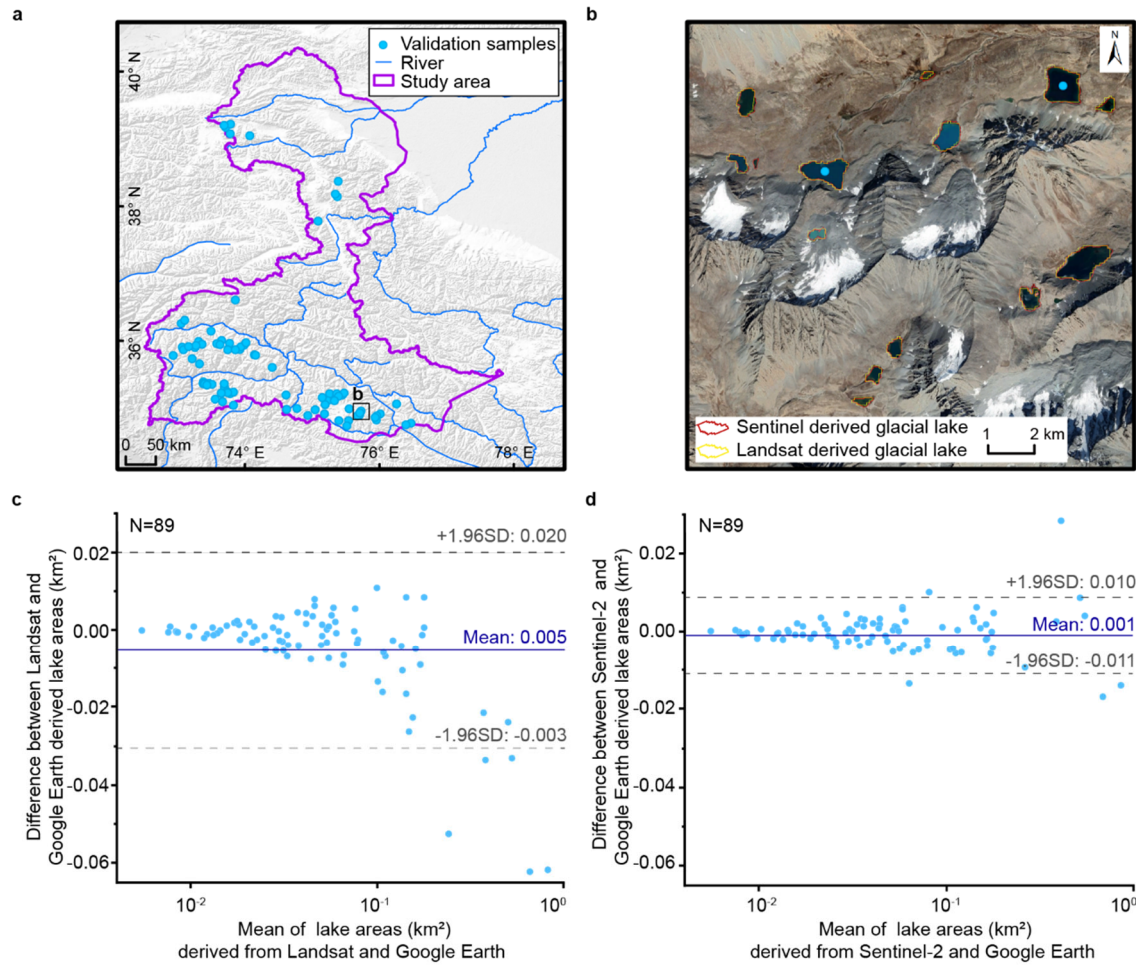
Figure 9. Distribution of validation samples (a), comparison of glacial lakes derived from Landsat and Sentinel-2 overlaying Google Earth image (© Google Earth 2019) in a zoomed site (b), and glacial lake product validated by Google Earth derived lake boundaries (c and d).

6.2 Comparison of Sentinel-2 and Landsat derived products

Glacial lakes from Landsat and Sentinel-2 images have a high consistency in number and area with overlap rates from approximately 86% to 94% for all lakes greater than 0.0045 km^2 (Table 4), indicating a good potential for coordinated utility with Landsat archived observation (Figure 10). Lake extents extracted from Landsat and Sentinel images match well for various types and sizes (Figure 10 and Figure 11, Table 4). The best consistency rate reaches 94% for the glacial lakes between 0.1 km^2 and 0.2 km^2. The difference in area of glacial lakes extracted from Landsat and Sentinel-2 images generally lies within the uncertainty ranges.

Landsat derived glacial lake   Sentinel derived glacial lake   0   400m
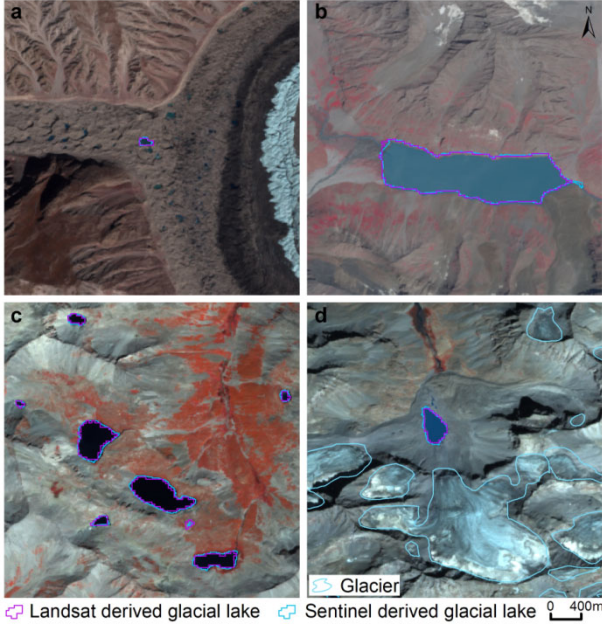
Figure 10. High consistency of lake extents extracted from Landsat and Sentinel-2 images. Lake types shown include supraglacial (a), glacier-fed moraine-dammed (b), unconnected glacial-erosion lake without glacier melt supply (c) and glacier-fed moraine-dammed lakes (d).

Spatial resolution of satellite images plays a primary role in the discrepancies in count and area of glacial lakes extracted from Landsat (30 m) and Sentinel-2 (10 m) observations. Due to a finer spatial resolution, Sentinel-2 images can extract more glacial lakes and more accurate extents than those from Landsat images. We set the same 5 pixels as the MMU for both Landsat and Sentinel-2 images, which corresponds to a minimum area of 0.0045 km^2 and 0.0005 km^2, respectively. The minimum mapping area results in generating nearly 5000 more lakes from Sentinel-2 images than from Landsat images, causing the greatest discrepancy in number (Table 4), such as Figure 11a. Small lakes such as supraglacial lakes play an important role in analyzing glacier evolution and supraglacial drainage systems (Liu and Mayer, 2015; Miles et al., 2018), implying a potential of our dataset to be applied in studies of glacier-lake evolutions. Meanwhile, Sentinel-2 images are able to depict boundaries of glacial lake with a lower uncertainty, as for some small islands and narrow channels (Figure 11b and c) were mapped from Sentinel-2 imagery that were unable to be detected in Landsat imagery.

Different acquisition dates between Sentinel-2 and Landsat images also contribute to the discrepancy of those two glacial lake data. Acquiring same-day images from the two sensors were not always possible due to the impacts of cloud contaminations, topographic shadows, snow cover and revisit periods (Williamson et al., 2018; Paul et al., 2020). Glacial lakes are changing temporally in the context of climate and glacier changes. The example is given to supraglacial lakes which showed considerable changes during a short period of time between the applied Landsat and Sentinel-2 images (Figure 11d). Despite our efforts of leveraging all available high-quality images, the overlap of acquisition dates between Landsat and Sentinel-2 images for the same location is relatively low (only 7 scenes of Sentinel-2 images or 112 glacial lakes in 2020) in this study area, and the consequential temporal gaps led to a

513   difference in the number and area of the derived glacial lakes.
514

515   □ Glacial lake derived from Landsat   □ Glacial lake derived from Sentinel-2
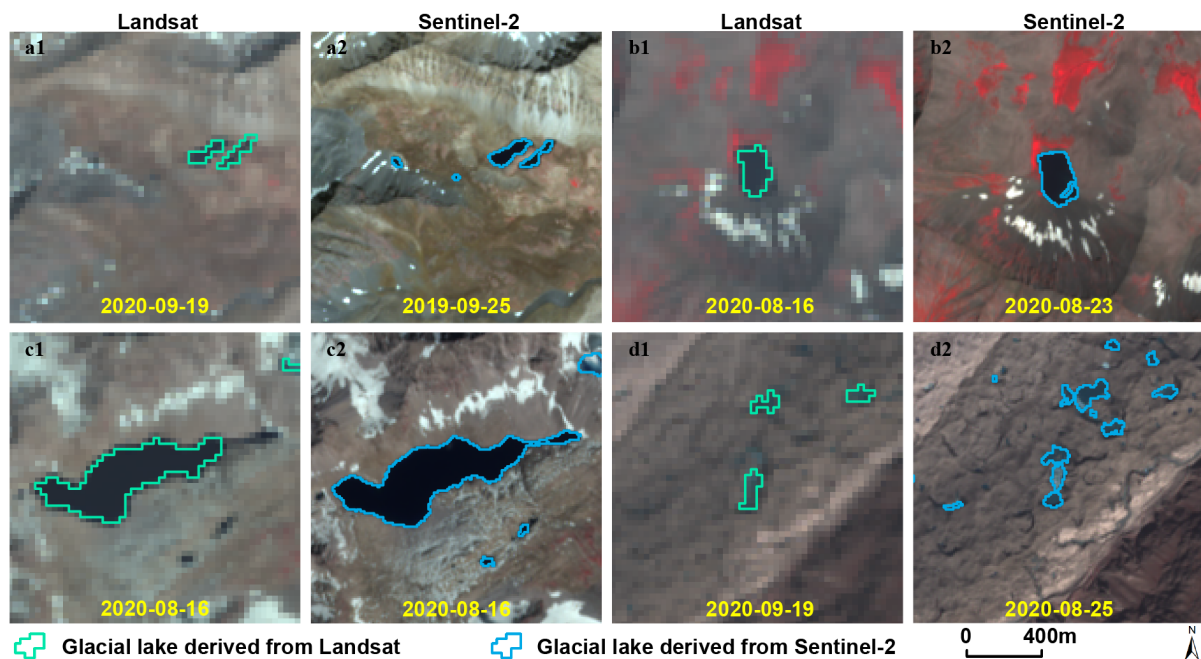
516   **Figure 11.** Discrepancy of lake extents extracted from Landsat and Sentinel-2 images.
517

518   6.3 Comparison with previous similar dataset

519   An increasing number of glacier lake datasets have been released over the past years, and
520   most of them were produced from long-term Landsat archives. Regional glacial lake datasets
521   using Sentinel images are scarce. Lack of Sentinel-derived glacial lake data in the study area
522   makes it impossible to compare. Here we selected four available glacial lake datasets to
523   compare with our Landsat-derived dataset.
524   We provide the latest glacial lake dataset (in 2020) and the most long-term 30-m Landsat
525   observation (1990 to 2020) for this study, with a range of critical attributes including two
526   types of classification systems. Within the same study area, our 2020 glacial lakes appear to
527   be closest to the 2018 dataset produced by Wang et al. (2020), with the highest overlap of
528   greater than 85% in area (Table 5). In Wang et al. (2020) , the minimum mapping unit is 6
529   pixels so their dataset has a less lake quantity. However, their dataset contains many large
530   landslide-dammed lakes that are excluded in our glacial lake mapping. As a result, their total
531   glacier lake area is greater than ours. The overlapping rates between Wang's glacial lakes
532   (2020) in 1990 and ours are more than 76% in area. However, their results show a distinct
533   increase of glacial lakes in number and area between 1990 and 2018 (Wang et al., 2020)
534   whereas our data show a more stable change between 1990 and 2020. One possible reason is
535   that manually delineating glacial lakes twice by different operators during Wang's lake
536   mapping (2020) exacerbates the errors of mapping. Another reason is that their data contains
537   landslide-dammed lakes that fluctuate greatly with time and expanded recently. One example
538   is the Attabad Lake (Located at 36°18'22.33"N, 74°49'34.36"E).
539
540

Table 5. Comparison of different glacial lake datasets sourced from Landsat images in the study area.

Baseline year (period)	Method	MMU m² (pixels)	Count (km²)	Other's area / ours (%)	Reference
1990 (1988-1993)	Manual	5400 (6)	1720 (89.68±13.69)	105.86	Wang et al., 2020
1990 (1990-1999)	Automated	50000 (55)	145 (20.28)	36.98	Shugar et al., 2020
1990 (1989-1992)	Manual	2700 (3)	622 (51.93±10.15)	61.02	Zhang et al., 2015
1990 (1989-1994)	*Semi-automated*	*4500 (5)*	*2154 (85.10±14.66)*	—	*This study*
2000 (1999-2001)	Manual	2700 (3)	724 (61.41±11.91)	71.32	Zhang et al., 2015
2000 (2000-2004)	Automated	50000 (55)	155 (22.35)	40.27	Shugar et al., 2020
2008	Automated & Manual	8100 (9)	1067 (65.45)	78.08	Chen et al., 2021
2000 (1996-2004)	*Semi-automated*	*4500 (5)*	*2184 (86.10±14.83)*	—	*This study*
2015 (2015-2018)	Automated	50000 (55)	148 (21.45)	38.77	Shugar et al., 2020
2017	Automated & Manual	8100 (9)	1063 (63.23)	75.47	Chen et al., 2021
2018 (2017-2018)	Manual	5400 (6)	1956 (102.46±15.48)	119.24	Wang et al., 2020
2020 (2016-2020)	*Semi-automated*	*4500 (5)*	*2234 (86.31±14.98)*	—	*This study*

Note: MMU represents minimum mapping units. The % represent the rate in area calculated by dividing individual glacial lake dataset by our Landsat-derived data greater than the same minimum lake size in the nearest baseline year respectively.

The second highest overlapping rate is approximate 54% for 2008 and 58% for 2017 in area comparing with Chen's data (Chen et al., 2021). Similarly, a minimum mapping unit of 55 pixels (50000 m²) in Shugar et al.'s, dataset (2020) led to the lowest overlap with less than 24% in area. The dataset from Zhang et al. (2015) shows fewer glacial lakes in 1990 and 2000 even with a smaller MMU of 3 pixels. By inspecting their dataset, we attributed this anomalous discrepancy to a range of glacial lakes that were missing due to lack of thorough cross-check quality assurance during their manual delineation. Our Landsat derived glacial lake dataset has been visually cross-checked over three time periods after the step of threshold-based semi-automated lake mapping, and also been visually validated by Sentinel-2 derived glacial lakes. Through this series of quality assurance, we aim at delivering one of the most reliable multi-decadal glacial lake products for this study area.

Other factors, such as image quality and acquisition dates, mapping methods and quality assurance workflow, might also lead to the discrepancies between the glacial lake datasets. Despite such discrepancies, an increasing number of publically-shared datasets benefit potential users to select the most suitable one for their objectives. Herein, we provide an up-to-date glacial lake dataset derived from both Landsat and Sentinel-2 observations, which further increased the availability of glacial lake dataset for water resource and GLOFs risk assessment, predicting glacier-lake evolutions (Carrivick et al., 2020) in the context of climate change.

6.4 Limitation and updating plan

We would like to acknowledge several limitations of our glacier lake dataset, largely due the availability of high quality satellite images in the study area and inadequate field survey data (Wang et al., 2020; Chen et al., 2021). First, it is unlikely to collect enough good-quality images within one calendar year for the entire study area due to high possibility of cloud or snow covers. Even though the capacity of repeat observations for Landsat-8 OLI and

Sentinel-2 increased (Roy et al., 2014; Williamson et al., 2018; Wulder et al., 2019; Paul et al., 2020), the 2020 glacial lake dataset has to employ images acquired in adjacent years besides 2020. Most images used from Landsat and Sentinel-2 platforms were imaged in autumn, and some images taken between April and July and in November also were employed. Distribution and changes in glacial lakes primarily represent the characteristics between August and October. Glacial lakes evolve with time and space (Nie et al., 2017), and subtle inter- and intra-annual changes (Liu et al., 2020) for each time period were ignored. Second, field investigation data are limited due to low accessibility of high mountain environment in the study area, which restrained the accuracy in classifying the glacial lake types. Although very high-resolution Google Earth images were utilized to assist in lake type interpretation, occasional misclassification was unavoidable. We implemented two types of classification systems based on a careful utilization of glacier data, DEM, geomorphological features and expert knowledge. However, the lack of in situ survey prohibited a thorough validation of the glacial lake types. Third, the rigorous quality assurance and cross check after semi-automated lake mapping assure the quality of our lake dataset but are still time and cost prohibitive. State-of-the-art mapping methods, such as deep learning method (Wu et al., 2020), Google Earth Engine cloud-computing (Chen et al., 2021) and synergy of SAR and optical images (Wangchuk and Bolch, 2020; How et al., 2021), would be used in the future to balance product accuracy and time cost.

The glacial lake dataset will be updated using newly collected Landsat and Sentinel images at a five-year interval or modified according to user feedbacks. The updated glacial lake dataset will continue to be released freely and publicly on the Mountain Science Data Center sharing platform.

7 Data availability

Our glacial lake dataset extracted from Sentinel-2 images in 2020 and Landsat observation between 1990 and 2020 are available online via the Mountain Science Data Center, the Institute of Mountain Hazards and Environment, the Chinese Academy of Sciences at https://doi.org/10.12380/Glaci.msdc.000001 (Lesi et al., 2022). The glacial lake dataset is provided in both ESRI shapefile format (total size of 22.6 MB) and the Geopackage format (version 1.2.1) with a total size of 9.2MB, which can be opened and further processed by open-source geographic information system software such as QGIS.

8 Conclusions

Glacial lake inventories of the entire China-Pakistan Economic Corridor in 2020 were provided based on Landsat and Sentinel-2 images using a threshold-based semi-automated mapping method. Both Landsat and Sentinel-2 derived glacial lake dataset show similar characteristics in spatial distribution and in the statistics of count and area. By contrast, glacial lake dataset derived from Sentinel-2 images with a spatial resolution of 10 m has a lower mapping error and more accurate lake boundary than those from 30 m spatial resolution Landsat images whereas Landsat imagery is more suitable to analyze spatial-temporal changes at a longer time scale due to its long-term archived observations at a consistent 30 m spatial resolution starting from the late 1980s.

Glacial lakes in the study area remain relatively stable with a slight increase in number and area between 1990 and 2020 according to Landsat observations. Our dataset reveals that 2154 glacial lakes in 1990 covering 85.1 ± 14.66 km^2 increased to 2234 lakes with a total area of 86.31 ± 14.98 km^2. The same mapping method and rigorous workflow of quality assurance and quality control used in this study reduced the error in multi-temporal changes of glacial lakes.

The Hanshaw's error estimation method for pixel-based lake mapping was improved by removing repeatedly calculated edge pixels that vary with lake shape. Therefore, the newly proposed method reduces the estimated value of uncertainty from satellite observations. The average relative error is $\pm 17.36\%$ for Landsat-derived product and $\pm 8.15\%$ for product from Sentinel-2.

Our glacial lake dataset contains a range of critical parameters that maximize their potential utility for water resource and GLOFs risk evaluation, cryosphere-hydrological and glacier-lake evolution projection. The dual classification systems of glacial lake types were developed and are very likely to attract broader researchers and scientists to use our datasets. In comparison with other existing glacial lake datasets, our products were created through a thorough consideration of lake types, cross checks and rigorous quality assurance, and will be updated and released continuously in the Mountain Science Data Center. As such, we expect that our glacial lake dataset will have significant value to cryospheric-hydrology research, the assessment of water resource and glacier-related hazards in the CPEC.

Appendix. The appendix related to this article is available online.

Author contributions. ML and YN conceived the study, ML, YN and XD performed data processing and analysis of the glacial lake inventory data, JW contributed to tool development and mapping methods, ML and YN wrote the manuscript. All authors reviewed and edited the manuscript before submission.

Competing interests. The authors declare no conflict of interest.

Acknowledgements.
We are grateful for the editor Kenneth Mankoff and three anonymous referees for their constructive comments that greatly help us to improve this manuscript. This study was supported by the second Tibetan Plateau Scientific Expedition and Research Program (grant 2019QZKK0603), the National Natural Science Foundation of China (Grant Nos. 42171086, 41971153), the International Science & Technology Cooperation Program of China (No. 2018YFE0100100), the Chinese Academy of Sciences "Light of West China" and Natural Sciences and Engineering Research Council of Canada (Grant No. DG-2020-04207).

651 **Appendix**

652 **Tutorial for Improved Uncertainty Estimating Method**

653

654 The Hanshaw's equation was originally proposed for pixelated polygons (such as a polygon
655 directly extracted from a remote sensing image), and performed more robustly than manually
656 digitized polygons (where vertices do not necessarily follow the pixel edges). Our improved
657 method also performs better for pixelated polygons. This tutorial is dedicated to helping
658 implement our improved uncertainty estimation method.

659

660 **Procedure of uncertainty estimating method (using ArcGIS (© ESRI) for example)**
661 1. Removing redundant nodes (optional)
662 We found that a small proportion (~1%) of the pixelated lake polygons (directly extracted
663 from satellite images) have redundant nodes, which affects the value of inner nodes. If no
664 redundant nodes exist, this step can be skipped. Or, we recommend using the "Simplify
665 Polygon" tool in ArcGIS to remove those nodes (Figure A1).
666   In the Simplify Polygon panel
667 ● Input your dataset.
668 ● Set the output path and output file name.
669 ● Choose the simplification algorithm. We recommended "POINT_REMOVE".
670 ● Set the tolerance of simplification algorithm. In this step, we need to ensure that the
671   polygon boundaries remain unchanged after deleting redundant nodes. Generally, a
672   tolerance of 1 meter will suffice, or you can adjust the threshold until your satisfaction.

673
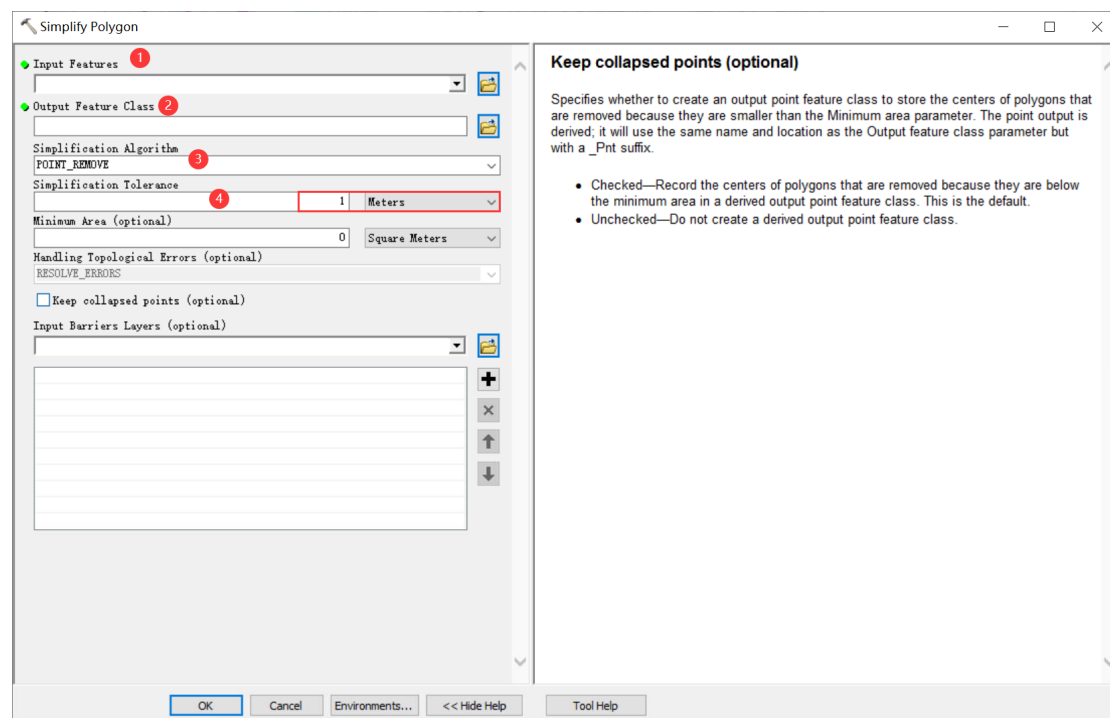
674 **Figure A1.** Input and option for Simplify Polygon in ArcGIS.

675

676 2. Calculating the total number of nodes using ArcGIS (Figure A2):
677 ● Add a new field in the attribute table of dataset.
678 ● Open Field Calculator.
679 ● Switch the parser to python mode, and enter the following code "!shape.pointcount!" in
680 the blue box to calculate the total number of nodes for each glacial lake boundary.
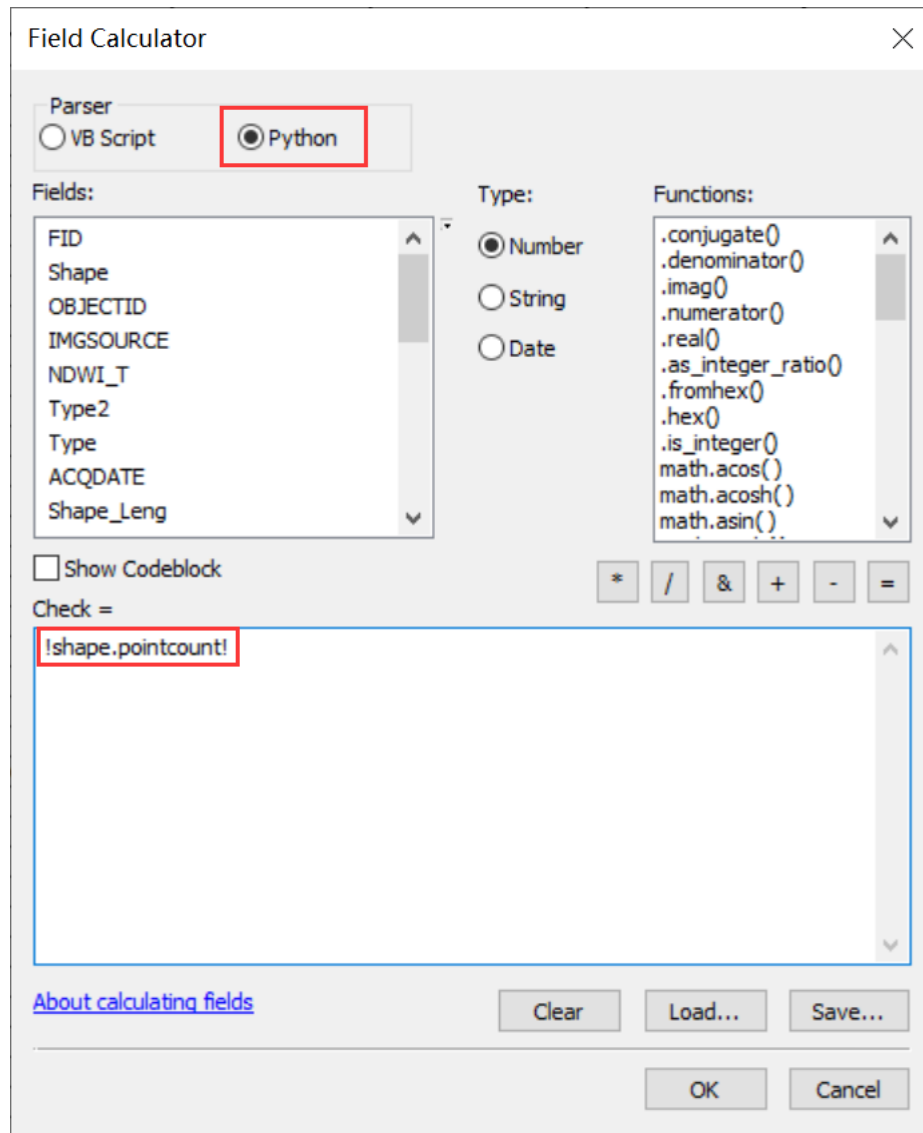
681
682 **Figure A2.** Total node calculation in ArcGIS.
683
684 3. Calculating the number of inner nodes:
685
686 For polygons without islands (Figure A3), use the equation 5. An inner node is a polygon
687 vertex where the interior angle surrounding it is greater than 180 degrees. An outer node is
688 the opposite of the inner node, where the interior angle is less than 180 degrees. We found
689 that the outer nodes are usually four more than the inner nodes in our glacial lake dataset. The
690 total nodes in ArcGIS contain one overlapping node to close the polygon, meaning the
691 endpoint is also the startpoint. This extra count was deleted in the calculation (equation 5).
692
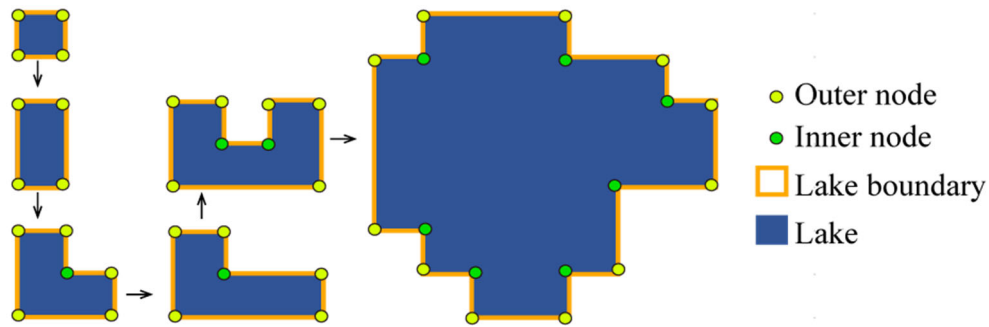
693
694 **Figure A3.** Sketch of outer and inner nodes of various glacial lakes without island.
695

696 For polygons with island (Figure A4) use the equation 6.
697
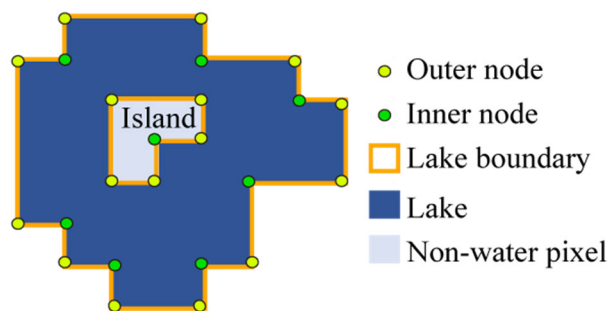
698
699 **Figure A4.** Sketch of outer and inner nodes for glacial lake with island.
700

701 We further specify the steps below to help implement equation 6.
702

703 Sept 1: detect the number of islands within each polygon.
704 ● Convert the initial lake polygon to polyline using the "Feature To Line" tool (Figure A5).
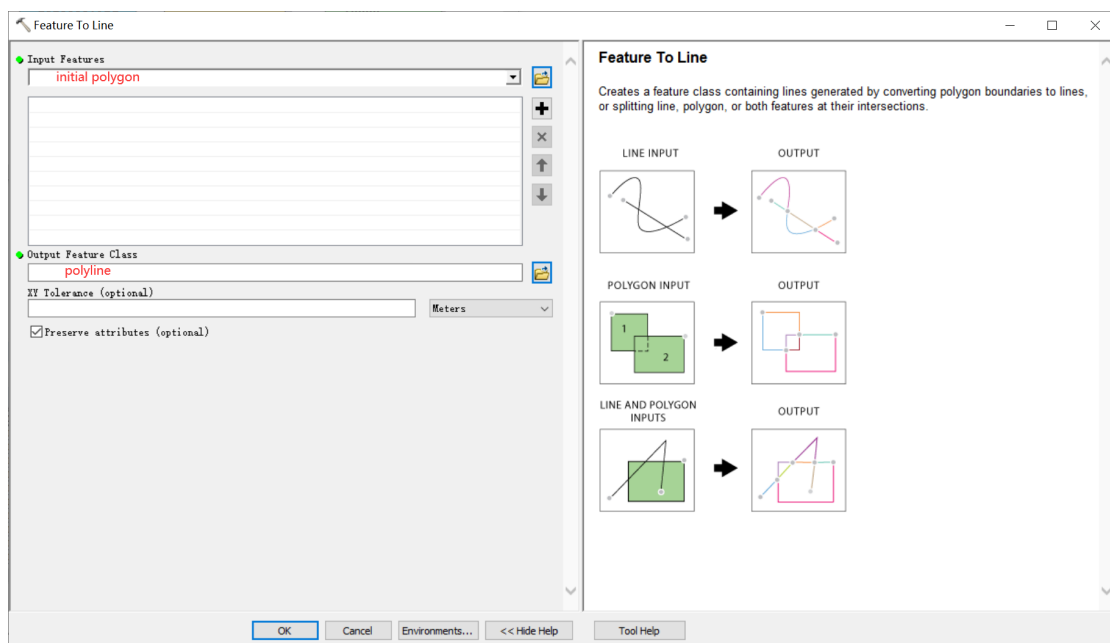
705
706 **Figure A5.** Feature To Line tool in ArcGIS
707

708   ●   Convert the polyline to generate a new polygon (Figure A6).

709
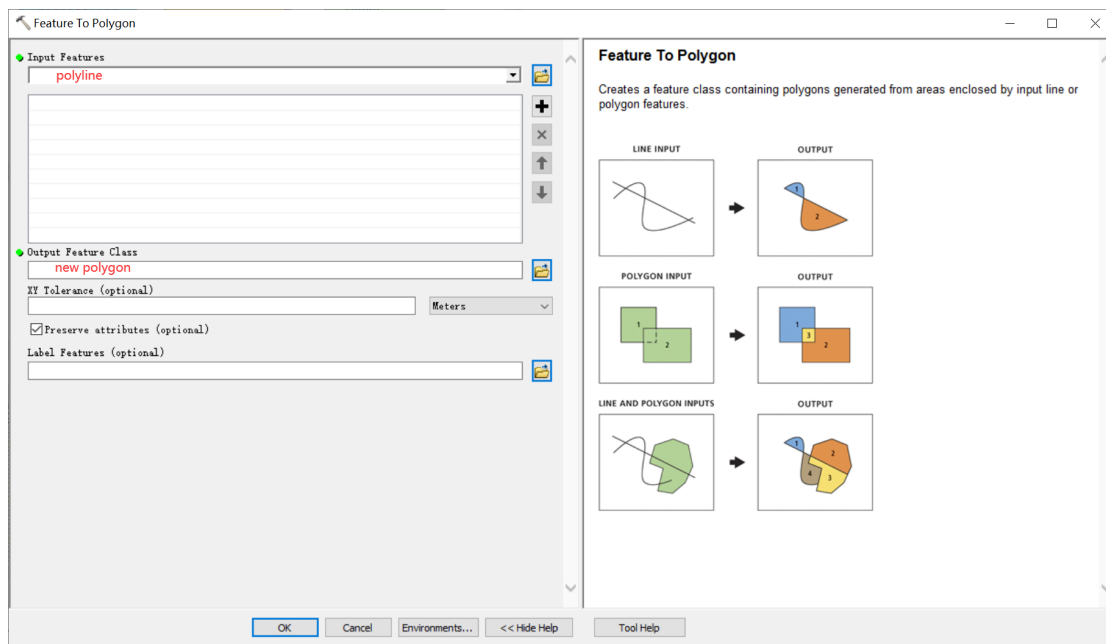
Figure A6. Feature To Polygon tool in ArcGIS

710

711

712   ●   Erase the new polygon by the initial polygon, which outputs the islands. Then we can
713   count how many islands there are in each lake (Figure A7).

714
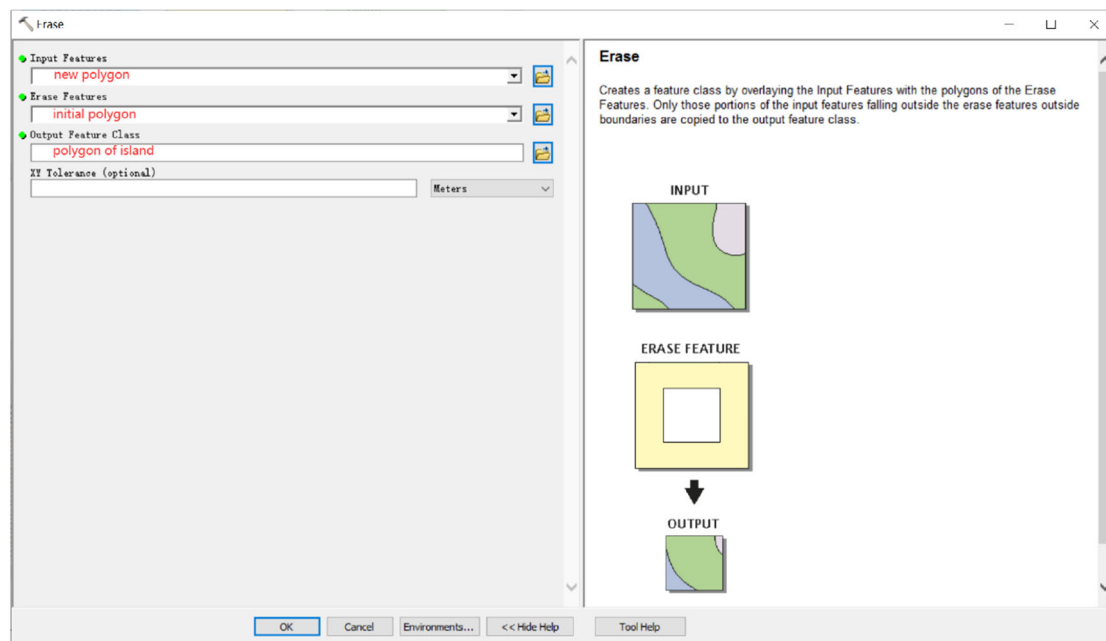
Figure A7. Erase tool in ArcGIS.

715

716

717 Step 2: calculate the number of inner nodes for each polygon with island using equation 6.

718

719 4. Calculating the uncertainty of lake mapping using equation 4.

720
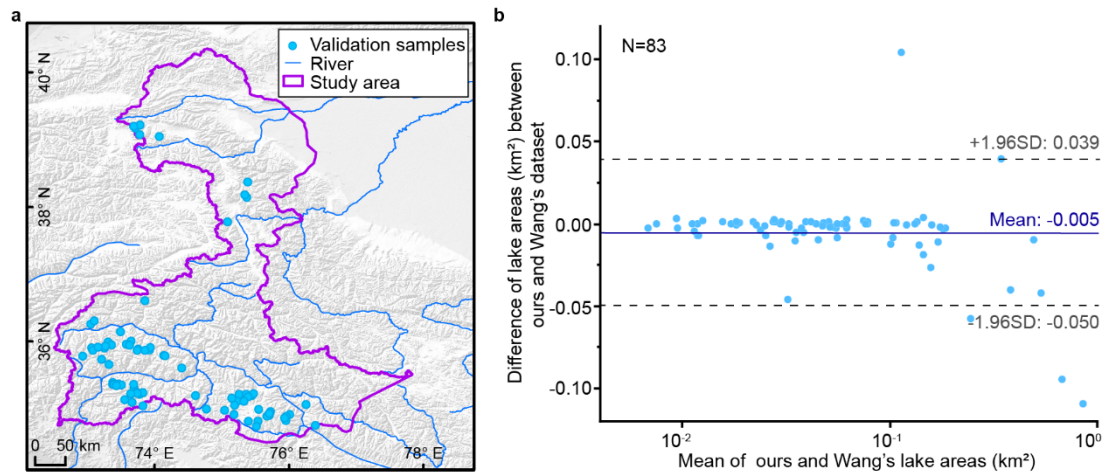
Figure A8. Distribution of validation samples (a) and comparison of glacial lakes (b) derived from our Landsat product in 2020 and Wang's lake data in 2018.

References

Ashraf, A., Naz, R., Iqbal, M.B.: Altitudinal dynamics of glacial lakes under changing climate in the Hindu

Kush, Karakoram, and Himalaya ranges. Geomorphology, 283: 72-79,

https://doi.org/10.1016/j.geomorph.2017.01.033, 2017.

Azam, M.F., Kargel, J.S., Shea, J.M., Nepal, S., Haritashya, U.K., Srivastava, S., Maussion, F., Qazi, N.,

Chevallier, P., Dimri, A.P., Kulkarni, A.V., Cogley, J.G., Bahuguna, I.: Glaciohydrology of the Himalaya-

Karakoram. Science, 373: eabf3668, https://doi.org/10.1126/science.abf3668, 2021.

Battamo, A.Y., Varis, O., Sun, P., Yang, Y., Oba, B.T., Zhao, L.: Mapping socio-ecological resilience along the

seven economic corridors of the Belt and Road Initiative. J. Clean. Prod., 309: 127341,

https://doi.org/10.1016/j.jclepro.2021.127341, 2021.

Bhambri, R., Hewitt, K., Kawishwar, P., Kumar, A., Verma, A., Snehmani, Tiwari, S., Misra, A.: Ice-dams,

outburst floods, and movement heterogeneity of glaciers, Karakoram. Global Planet. Change, 180: 100-116,

https://doi.org/10.1016/j.gloplacha.2019.05.004, 2019.

738 Bhattacharya, A., Bolch, T., Mukherjee, K., King, O., Menounos, B., Kapitsa, V., Neckel, N., Yang, W., Yao,

739 T.: High Mountain Asian glacier response to climate revealed by multi-temporal satellite observations since the

740 1960s. Nat. Commun., 12: 4133, https://doi.org/10.1038/s41467-021-24180-y, 2021.

741 Bolch, T., Pieczonka, T., Mukherjee, K., Shea, J.: Brief communication: Glaciers in the Hunza catchment

742 (Karakoram) have been nearly in balance since the 1970s. The Cryosphere, 11: 531-539,

743 https://doi.org/10.5194/tc-11-531-2017, 2017.

744 Brun, F., Berthier, E., Wagnon, P., Kääb, A., Treichler, D.: A spatially resolved estimate of High Mountain Asia

745 glacier mass balances from 2000 to 2016. Nat. Geosci., 10: 668-673, https://doi.org/10.1038/ngeo2999, 2017.

746 Brun, F., Wagnon, P., Berthier, E., Jomelli, V., Maharjan, S.B., Shrestha, F., Kraaijenbrink, P.D.A.:

747 Heterogeneous Influence of Glacier Morphology on the Mass Balance Variability in High Mountain Asia.

748 Journal of Geophysical Research: Earth Surface, 124: 1331-1345, https://doi.org/10.1029/2018JF004838, 2019.

749 Carrivick, J.L., Tweed, F.S.: Proglacial lakes: character, behaviour and geological importance. Quaternary Sci.

750 Rev., 78: 34-52, https://doi.org/10.1016/j.quascirev.2013.07.028, 2013.

751 Carrivick, J.L., Quincey, D.J.: Progressive increase in number and volume of ice-marginal lakes on the western

752 margin of the Greenland Ice Sheet. Global Planet. Change, 116: 156-163,

753 https://doi.org/10.1016/j.gloplacha.2014.02.009, 2014.

754 Carrivick, J.L., Tweed, F.S.: A global assessment of the societal impacts of glacier outburst floods. Global

755 Planet. Change, 144: 1-16, https://doi.org/10.1016/j.gloplacha.2016.07.001, 2016.

756 Carrivick, J.L., Tweed, F.S., Sutherland, J.L., Mallalieu, J.: Toward Numerical Modeling of Interactions

757 Between Ice-Marginal Proglacial Lakes and Glaciers. Frontiers in Earth Science, 8,

758 https://doi.org/10.3389/feart.2020.577068, 2020.

759   Carrivick, J.L., How, P., Lea, J.M., Sutherland, J.L., Grimes, M., Tweed, F.S., Cornford, S., Quincey, D.J.,

760   Mallalieu, J.: Ice-Marginal Proglacial Lakes Across Greenland: Present Status and a Possible Future. Geophys.

761   Res. Lett., 49: e2022GL099276, https://doi.org/https://doi.org/10.1029/2022GL099276, 2022.

762   Chen, F., Zhang, M., Guo, H., Allen, S., Kargel, J.S., Haritashya, U.K., Watson, C.S.: Annual 30 m dataset for

763   glacial lakes in High Mountain Asia from 2008 to 2017. Earth System Science Data, 13: 741-766,

764   https://doi.org/10.5194/essd-13-741-2021, 2021.

765   Chen, X., Cui, P., You, Y., Cheng, Z., Khan, A., Ye, C., Zhang, S.: Dam-break risk analysis of the Attabad

766   landslide dam in Pakistan and emergency countermeasures. Landslides, 14: 675-683,

767   https://doi.org/10.1007/s10346-016-0721-7, 2017.

768   Cook, S.J., Quincey, D.J.: Estimating the volume of Alpine glacial lakes. Earth Surf. Dynam., 3: 559-575,

769   https://doi.org/10.5194/esurf-3-559-2015, 2015.

770   Emmer, A., Cuřín, V.: Can a dam type of an alpine lake be derived from lake geometry? A negative result. J.

771   Mt. Sci.-Engl., 18: 614-621, https://doi.org/10.1007/s11629-020-6003-9, 2021.

772   Farr, T.G., Rosen, P.A., Caro, E., Crippen, R., Duren, R., Hensley, S., Kobrick, M., Paller, M., Rodriguez, E.,

773   Roth, L., Seal, D., Shaffer, S., Shimada, J., Umland, J., Werner, M., Oskin, M., Burbank, D., Alsdorf, D.: The

774   Shuttle Radar Topography Mission. Rev. Geophys., 45: RG2004, https://doi.org/10.1029/2005RG000183, 2007.

775   Gardelle, J., Arnaud, Y., Berthier, E.: Contrasted evolution of glacial lakes along the Hindu Kush Himalaya

776   mountain range between 1990 and 2009. Global Planet. Change, 75: 47-55,

777   https://doi.org/10.1016/j.gloplacha.2010.10.003, 2011.

778   Hanshaw, M.N., Bookhagen, B.: Glacial areas, lake areas, and snow lines from 1975 to 2012: status of the

779   Cordillera Vilcanota, including the Quelccaya Ice Cap, northern central Andes, Peru. The Cryosphere, 8: 359-

780   376, https://doi.org/10.5194/tc-8-359-2014, 2014.

781 Hewitt, K.: The Karakoram Anomaly? Glacier Expansion and the 'Elevation Effect,' Karakoram Himalaya. Mt.

782 Res. Dev., 25: 332-340, https://doi.org/10.1659/0276-4741(2005)025[0332:TKAGEA]2.0.CO;2, 2005.

783 Hewitt, K., 2014. Glaciers of the Karakoram Himalaya: Glacial Environments, Processes, Hazards and

784 Resources. Springer, Dordrecht.

785 How, P., Messerli, A., Mätzler, E., Santoro, M., Wiesmann, A., Caduff, R., Langley, K., Bojesen, M.H., Paul,

786 F., Kääb, A., Carrivick, J.L.: Greenland-wide inventory of ice marginal lakes using a multi-method approach.

787 Sci. Rep.-UK, 11: 4481, https://doi.org/10.1038/s41598-021-83509-1, 2021.

788 Huggel, C., Kääb, A., Haeberli, W., Teysseire, P., Paul, F.: Remote sensing based assessment of hazards from

789 glacier lake outbursts: a case study in the Swiss Alps. Can. Geotech. J., 39: 316-330,

790 https://doi.org/10.1139/t01-099, 2002.

791 Hugonnet, R., Mcnabb, R., Berthier, E., Menounos, B., Nuth, C., Girod, L., Farinotti, D., Huss, M., Dussaillant,

792 I., Brun, F., Kääb, A.: Accelerated global glacier mass loss in the early twenty-first century. Nature, 592: 726-

793 731, https://doi.org/10.1038/s41586-021-03436-z, 2021.

794 Huss, M., Hock, R.: Global-scale hydrological response to future glacier mass loss. Nat. Clim. Change, 8: 135-

795 140, https://doi.org/10.1038/s41558-017-0049-x, 2018.

796 Immerzeel, W.W., Lutz, A.F., Andrade, M., Bahl, A., Biemans, H., Bolch, T., Hyde, S., Brumby, S., Davies,

797 B.J., Elmore, A.C., Emmer, A., Feng, M., Fernández, A., Haritashya, U., Kargel, J.S., Koppes, M.,

798 Kraaijenbrink, P.D.A., Kulkarni, A.V., Mayewski, P.A., Nepal, S., Pacheco, P., Painter, T.H., Pellicciotti, F.,

799 Rajaram, H., Rupper, S., Sinisalo, A., Shrestha, A.B., Viviroli, D., Wada, Y., Xiao, C., Yao, T., Baillie, J.E.M.:

800 Importance and vulnerability of the world's water towers. Nature, 577: 364-369, https://doi.org/10.1038/s41586-

801 019-1822-y, 2020.

802   Jarvis, A., Reuter, H.I., Nelson, A., Guevara, E., 2008. Hole-filled seamless SRTM data V4. 2008, International

803   Centre for Tropical Agriculture (CIAT), available from http://srtm.csi.cgiar.org.

804   Jiang, S., Nie, Y., Liu, Q., Wang, J., Liu, L., Hassan, J., Liu, X., Xu, X.: Glacier Change, Supraglacial Debris

805   Expansion and Glacial Lake Evolution in the Gyirong River Basin, Central Himalayas, between 1988 and 2015.

806   Remote Sens.-Basel, 10: 986, https://doi.org/10.3390/rs10070986, 2018.

807   Kääb, A., Berthier, E., Nuth, C., Gardelle, J., Arnaud, Y.: Contrasting patterns of early twenty-first-century

808   glacier mass change in the Himalayas. Nature, 488: 495-498, https://doi.org/10.1038/nature11324, 2012.

809   Lesi, M., Nie, Y., Shugar, D.H., Wang, J., Deng, Q., Chen, H.: Landsat and Sentinel-derived glacial lake dataset

810   in the China-Pakistan Economic Corridor from 1990 to 2020. Mountain Science Data Center,

811   https://doi.org/10.12380/Glaci.msdc.000001   CSTR:1a006.11.Glaci.msdc.000001, 2022.

812   Li, D., Shangguan, D., Anjum, M.N.: Glacial Lake Inventory Derived from Landsat 8 OLI in 2016–2018 in

813   China–Pakistan Economic Corridor. ISPRS international journal of geo-information, 9: 294,

814   https://doi.org/10.3390/ijgi9050294, 2020.

815   Li, Z., Deng, X., Zhang, Y.: Evaluation and convergence analysis of socio-economic vulnerability to natural

816   hazards of Belt and Road Initiative countries. J. Clean. Prod., 282: 125406,

817   https://doi.org/10.1016/j.jclepro.2020.125406, 2021.

818   Liu, Q., Mayer, C.: Distribution and interannual variability of supraglacial lakes on debris-covered glaciers in

819   the Khan Tengri-Tumor Mountains, Central Asia. Environ. Res. Lett., 10: 014014 2015.

820   Liu, Q., Mayer, C., Wang, X., Nie, Y., Wu, K., Wei, J., Liu, S.: Interannual flow dynamics driven by frontal

821   retreat of a lake-terminating glacier in the Chinese Central Himalaya. Earth Planet. Sc. Lett., 546: 116450,

822   https://doi.org/10.1016/j.epsl.2020.116450, 2020.

823   Lyons, E.A., Sheng, Y., Smith, L.C., Li, J., Hinkel, K.M., Lenters, J.D., Wang, J.: Quantifying sources of error

824   in multitemporal multisensor lake mapping. Int. J. Remote Sens., 34: 7887-7905,

825   https://doi.org/10.1080/01431161.2013.827343, 2013.

826   Martín, C.N.S., Ponce, J.F., Montes, A., Balocchi, L.D., Gorza, C., Andrea, C.: Proglacial landform assemblage

827   in a rapidly retreating cirque glacier due to temperature increase since 1970, Fuegian Andes, Argentina.

828   Geomorphology, 390: 107861, https://doi.org/10.1016/j.geomorph.2021.107861, 2021.

829   Maurer, J.M., Schaefer, J.M., Rupper, S., Corley, A.: Acceleration of ice loss across the Himalayas over the past

830   40 years. Science Advances, 5: eaav7266, https://doi.org/10.1126/sciadv.aav7266, 2019.

831   Mcfeeters, S.K.: The use of the Normalized Difference Water Index (NDWI) in the delineation of open water

832   features. Int. J. Remote Sens., 17: 1425 - 1432 1996.

833   Miles, E.S., Watson, C.S., Brun, F., Berthier, E., Esteves, M., Quincey, D.J., Miles, K.E., Hubbard, B., Wagnon,

834   P.: Glacial and geomorphic effects of a supraglacial lake drainage and outburst event, Everest region, Nepal

835   Himalaya. The Cryosphere, 12: 3891-3905, https://doi.org/10.5194/tc-12-3891-2018, 2018.

836   Nie, Y., Zhang, Y., Liu, L., Zhang, J.: Glacial change in the vicinity of Mt. Qomolangma (Everest), central high

837   Himalayas since 1976. J. Geogr. Sci., 20: 667-686, https://doi.org/10.1007/s11442-010-0803-8, 2010.

838   Nie, Y., Sheng, Y., Liu, Q., Liu, L., Liu, S., Zhang, Y., Song, C.: A regional-scale assessment of Himalayan

839   glacial lake changes using satellite observations from 1990 to 2015. Remote Sens. Environ., 189: 1-13,

840   https://doi.org/10.1016/j.rse.2016.11.008, 2017.

841   Nie, Y., Liu, Q., Wang, J., Zhang, Y., Sheng, Y., Liu, S.: An inventory of historical glacial lake outburst floods

842   in the Himalayas based on remote sensing observations and geomorphological analysis. Geomorphology, 308:

843   91-106, https://doi.org/10.1016/j.geomorph.2018.02.002, 2018.

844   Nie, Y., Liu, W., Liu, Q., Hu, X., Westoby, M.J.: Reconstructing the Chongbaxia Tsho glacial lake outburst

845   flood in the Eastern Himalaya: Evolution, process and impacts. Geomorphology, 370: 107393,

846   https://doi.org/10.1016/j.geomorph.2020.107393, 2020.

847   Nie, Y., Pritchard, H.D., Liu, Q., Hennig, T., Wang, W., Wang, X., Liu, S., Nepal, S., Samyn, D., Hewitt, K.,

848   Chen, X.: Glacial change and hydrological implications in the Himalaya and Karakoram. Nature Reviews Earth

849   & Environment, 2: 91-106, https://doi.org/10.1038/s43017-020-00124-w, 2021.

850   Paul, F., Rastner, P., Azzoni, R.S., Diolaiuti, G., Fugazza, D., Le Bris, R., Nemec, J., Rabatel, A., Ramusovic,

851   M., Schwaizer, G., Smiraglia, C.: Glacier shrinkage in the Alps continues unabated as revealed by a new glacier

852   inventory from Sentinel-2. Earth System Science Data, 12: 1805-1821, https://doi.org/10.5194/essd-12-1805-

853   2020, 2020.

854   Pfeffer, W.T., Arendt, A.A., Bliss, A., Bolch, T., Cogley, J.G., Gardner, A.S., Hagen, J., Hock, R., Kaser, G.,

855   Kienholz, C., Miles, E.S., Moholdt, G., Mölg, N., Paul, F., Radić, V., Rastner, P., Raup, B.H., Rich, J., Sharp,

856   M.J.: The Randolph Glacier Inventory: a globally complete inventory of glaciers. J. Glaciol., 60: 537-552,

857   https://doi.org/10.3189/2014JoG13J176, 2014.

858   Post, A., Mayo, L.R., 1971. Glacier dammed lakes and outburst floods in Alaska: U.S. Geological Survey

859   Hydrologic Investigations Atlas 455, U.S. Geological Survey.

860   Pritchard, H.D.: Asia's shrinking glaciers protect large populations from drought stress. Nature, 569: 649-654,

861   https://doi.org/10.1038/s41586-019-1240-1, 2019.

862   Quincey, D.J., Richardson, S.D., Luckman, A., Lucas, R.M., Reynolds, J.M., Hambrey, M.J., Glasser, N.F.:

863   Early recognition of glacial lake hazards in the Himalaya using remote sensing datasets. Global Planet. Change,

864   56: 137-152, https://doi.org/10.1016/j.gloplacha.2006.07.013, 2007.

865   Rabus, B., Eineder, M., Roth, A., Bamler, R.: The shuttle radar topography mission—a new class of digital

866   elevation models acquired by spaceborne radar. ISPRS J. Photogramm., 57: 241-262,

867   https://doi.org/10.1016/S0924-2716(02)00124-7, 2003.

868   RGI Consortium: Randolph Glacier Inventory – A Dataset of Global Glacier Outlines: Version 6.0: Technical

869   Report, https://doi.org/10.7265/N5-RGI-60, 2017.

870   Rick, B., Mcgrath, D., Armstrong, W., Mccoy, S.W.: Dam type and lake location characterize ice-marginal lake

871   area change in Alaska and NW Canada between 1984 and 2019. The Cryosphere, 16: 297-314,

872   https://doi.org/10.5194/tc-16-297-2022, 2022.

873   Rose, A., Mckee, J., Sims, K., Bright, E., Reith, A., Urban, M.: LandScan Global 2020,

874   https://doi.org/https://doi.org/10.48690/1523378, 2021.

875   Rounce, D.R., Hock, R., Shean, D.E.: Glacier Mass Change in High Mountain Asia Through 2100 Using the

876   Open-Source Python Glacier Evolution Model (PyGEM). Frontiers in Earth Science, 7: 331,

877   https://doi.org/10.3389/feart.2019.00331, 2020.

878   Roy, D.P., Wulder, M.A., Loveland, T.R., C. E., W., Allen, R.G., Anderson, M.C., Helder, D., Irons, J.R.,

879   Johnson, D.M., Kennedy, R., Scambos, T.A., Schaaf, C.B., Schott, J.R., Sheng, Y., Vermote, E.F., Belward,

880   A.S., Bindschadler, R., Cohen, W.B., Gao, F., Hipple, J.D., Hostert, P., Huntington, J., Justice, C.O., Kilic, A.,

881   Kovalskyy, V., Lee, Z.P., Lymburner, L., Masek, J.G., Mccorkel, J., Shuai, Y., Trezza, R., Vogelmann, J.,

882   Wynne, R.H., Zhu, Z.: Landsat-8: Science and product vision for terrestrial global change research. Remote

883   Sens. Environ., 145: 154-172, https://doi.org/10.1016/j.rse.2014.02.001, 2014.

884   Sakai, A.: Brief communication: Updated GAMDAM glacier inventory over high-mountain Asia. The

885   Cryosphere, 13: 2043-2049, https://doi.org/10.5194/tc-13-2043-2019, 2019.

886   Salerno, F., Thakuri, S., D'Agata, C., Smiraglia, C., Manfredi, E.C., Viviano, G., Tartari, G.: Glacial lake

887   distribution in the Mount Everest region: Uncertainty of measurement and conditions of formation. Global

888   Planet. Change, 92-93: 30-39 2012.

889   Shean, D.E., Bhushan, S., Montesano, P., Rounce, D.R., Arendt, A., Osmanoglu, B.: A Systematic, Regional

890   Assessment of High Mountain Asia Glacier Mass Balance. Frontiers in Earth Science, 7: 363,

891   https://doi.org/10.3389/feart.2019.00363, 2020.

892   Sheng, Y., Song, C., Wang, J., Lyons, E.A., Knox, B.R., Cox, J.S., Gao, F.: Representative lake water extent

893   mapping at continental scales using multi-temporal Landsat-8 imagery. Remote Sens. Environ., 185: 129-141,

894   https://doi.org/10.1016/j.rse.2015.12.041, 2016.

895   Shugar, D.H., Burr, A., Haritashya, U.K., Kargel, J.S., Watson, C.S., Kennedy, M.C., Bevington, A.R., Betts,

896   R.A., Harrison, S., Strattman, K.: Rapid worldwide growth of glacial lakes since 1990. Nat. Clim. Change, 10:

897   939-945, https://doi.org/10.1038/s41558-020-0855-4, 2020.

898   Shugar, D.H., Jacquemart, M., Shean, D., Bhushan, S., Upadhyay, K., Sattar, A., Schwanghart, W., Mcbride, S.,

899   de Vries, M., Mergili, M., Emmer, A., Deschamps-Berger, C., Mcdonnell, M., Bhambri, R., Allen, S., Berthier,

900   E., Carrivick, J.L., Clague, J.J., Dokukin, M., Dunning, S.A., Frey, H., Gascoin, S., Haritashya, U.K., Huggel,

901   C., Kaab, A., Kargel, J.S., Kavanaugh, J.L., Lacroix, P., Petley, D., Rupper, S., Azam, M.F., Cook, S.J., Dimri,

902   A.P., Eriksson, M., Farinotti, D., Fiddes, J., Gnyawali, K.R., Harrison, S., Jha, M., Koppes, M., Kumar, A.,

903   Leinss, S., Majeed, U., Mal, S., Muhuri, A., Noetzli, J., Paul, F., Rashid, I., Sain, K., Steiner, J., Ugalde, F.,

904   Watson, C.S., Westoby, M.J.: A massive rock and ice avalanche caused the 2021 disaster at Chamoli, Indian

905   Himalaya. Science, 373: 300-306, https://doi.org/10.1126/science.abh4455, 2021.

906   Ullah, S., You, Q., Ali, A., Ullah, W., Jan, M.A., Zhang, Y., Xie, W., Xie, X.: Observed changes in maximum

907   and minimum temperatures over China- Pakistan economic corridor during 1980–2016. Atmos. Res., 216: 37-

908   51, https://doi.org/10.1016/j.atmosres.2018.09.020, 2019.

909   Viviroli, D., Kummu, M., Meybeck, M., Kallio, M., Wada, Y.: Increasing dependence of lowland populations

910   on mountain water resources. Nature Sustainability, 3: 917-928, https://doi.org/10.1038/s41893-020-0559-9,

911   2020.

912   Wang, J., Sheng, Y., Tong, T.S.D.: Monitoring decadal lake dynamics across the Yangtze Basin downstream of

913   Three Gorges Dam. Remote Sens. Environ., 152: 251-269, https://doi.org/10.1016/j.rse.2014.06.004, 2014.

914   Wang, J., Sheng, Y., Wada, Y.: Little impact of the Three Gorges Dam on recent decadal lake decline across

915   China's Yangtze Plain. Water Resour. Res., 53: 3854-3877, https://doi.org/10.1002/2016WR019817, 2017.

916   Wang, J., Song, C., Reager, J.T., Yao, F., Famiglietti, J.S., Sheng, Y., Macdonald, G.M., Brun, F., Schmied,

917   H.M., Marston, R.A., Wada, Y.: Recent global decline in endorheic basin water storages. Nat. Geosci., 11: 926-

918   932, https://doi.org/10.1038/s41561-018-0265-7, 2018.

919   Wang, X., Ding, Y., Liu, S., Jiang, L., Wu, K., Jiang, Z., Guo, W.: Changes of glacial lakes and implications in

920   Tian Shan, Central Asia, based on remote sensing data from 1990 to 2010. Environ. Res. Lett., 8: 44052,

921   https://doi.org/10.1088/1748-9326/8/4/044052, 2013.

922   Wang, X., Liu, S., Zhang, J.: A new look at roles of the cryosphere in sustainable development. Advances in

923   Climate Change Research, 10: 124-131, https://doi.org/10.1016/j.accre.2019.06.005, 2019.

924   Wang, X., Guo, X., Yang, C., Liu, Q., Wei, J., Zhang, Y., Liu, S., Zhang, Y., Jiang, Z., Tang, Z.: Glacial lake

925   inventory of high-mountain Asia in 1990 and 2018 derived from Landsat images. Earth System Science Data,

926   12: 2169-2182, https://doi.org/10.5194/essd-12-2169-2020, 2020.

927 Wangchuk, S., Bolch, T.: Mapping of glacial lakes using Sentinel-1 and Sentinel-2 data and a random forest

928 classifier: Strengths and challenges. Science of Remote Sensing, 2: 100008,

929 https://doi.org/https://doi.org/10.1016/j.srs.2020.100008, 2020.

930 Westoby, M.J., Glasser, N.F., Brasington, J., Hambrey, M.J., Quincey, D.J., Reynolds, J.M.: Modelling outburst

931 floods from moraine-dammed glacial lakes. Earth-Sci. Rev., 134: 137-159,

932 https://doi.org/10.1016/j.earscirev.2014.03.009, 2014.

933 Williamson, A.G., Banwell, A.F., Willis, I.C., Arnold, N.S.: Dual-satellite (Sentinel-2 and Landsat 8) remote

934 sensing of supraglacial lakes in Greenland. The Cryosphere, 12: 3045-3065, https://doi.org/10.5194/tc-12-3045-

935 2018, 2018.

936 Wu, R., Liu, G., Zhang, R., Wang, X., Li, Y., Zhang, B., Cai, J., Xiang, W.: A Deep Learning Method for

937 Mapping Glacial Lakes from the Combined Use of Synthetic-Aperture Radar and Optical Satellite Images.

938 Remote Sens.-Basel, 12: 4020

939 2020.

940 Wulder, M.A., Loveland, T.R., Roy, D.P., Crawford, C.J., Masek, J.G., Woodcock, C.E., Allen, R.G.,

941 Anderson, M.C., Belward, A.S., Cohen, W.B., Dwyer, J., Erb, A., Gao, F., Griffiths, P., Helder, D., Hermosilla,

942 T., Hipple, J.D., Hostert, P., Hughes, M.J., Huntington, J., Johnson, D.M., Kennedy, R., Kilic, A., Li, Z.,

943 Lymburner, L., Mccorkel, J., Pahlevan, N., Scambos, T.A., Schaaf, C., Schott, J.R., Sheng, Y., Storey, J.,

944 Vermote, E., Vogelmann, J., White, J.C., Wynne, R.H., Zhu, Z.: Current status of Landsat program, science, and

945 applications. Remote Sens. Environ., 225: 127-147, https://doi.org/https://doi.org/10.1016/j.rse.2019.02.015,

946 2019.

947 Yao, C., Wang, X., Zhao, X., Wei, J., Zhang, Y.: Temporal and Spatial Changes of Glacial Lakes in the China-

948 Pakistan Economic Corridor from 1990 to 2018. Journal of Glaciology and Geocryology, 42: 33-42,

949 https://doi.org/https://doi.org/10.7522/j.issn.1000-0240.2020.0009, 2020.

950 Yao, T., Thompson, L., Yang, W., Yu, W.S., Gao, Y., Guo, X.J., Yang, X.X., Duan, K.Q., Zhao, H.B., Xu,

951 B.Q., Pu, J.C., Lu, A.X., Xiang, Y., Kattel, D.B., Joswiak, D.: Different glacier status with atmospheric

952 circulations in Tibetan Plateau and surroundings. Nat. Clim. Change, 2: 663-667,

953 https://doi.org/10.1038/NCLIMATE1580, 2012.

954 Yao, X., Liu, S., Han, L., Sun, M., Zhao, L.: Definition and classification system of glacial lake for inventory

955 and hazards study. J. Geogr. Sci., 28: 193-205, https://doi.org/10.1007/s11442-018-1467-z, 2018.

956 Zhang, G., Yao, T., Xie, H., Wang, W., Yang, W.: An inventory of glacial lakes in the Third Pole region and

957 their changes in response to global warming. Global Planet. Change, 131: 148-157,

958 https://doi.org/10.1016/j.gloplacha.2015.05.013, 2015.

959 Zhang, M., Chen, F., Tian, B.: An automated method for glacial lake mapping in High Mountain Asia using

960 Landsat 8 imagery. J. Mt. Sci.-Engl., 15: 13-24, https://doi.org/10.1007/s11629-017-4518-5, 2018.

961 Zhao, W., Xiong, D., Wen, F., Wang, X.: Lake area monitoring based on land surface temperature in the Tibetan

962 Plateau from 2000 to 2018. Environ. Res. Lett., 15, https://doi.org/10.1088/1748-9326/ab9b41, 2020.

963 Zheng, G., Allen, S.K., Bao, A., Ballesteros-Cánovas, J.A., Huss, M., Zhang, G., Li, J., Yuan, Y., Jiang, L., Yu,

964 T., Chen, W., Stoffel, M.: Increasing risk of glacial lake outburst floods from future Third Pole deglaciation.

965 Nat. Clim. Change, 11: 411-417, https://doi.org/10.1038/s41558-021-01028-3, 2021.

966